K. S. Thygesen[1] and A. Rubio[2]

[1]Center for Atomic-scale Materials Design (CAMD), Department of Physics, Technical University of Denmark, 2850 Kgs. Lyngby, Denmark
[2]Nano Bio Spectroscopy Group and European Theoretical Spectroscopy Facility (ETSF). Departamento de Fisica de Materiales, Unidad de Materiales Centro Mixto CSIC-UPV/EHU Universidad del Pas Vasco, Edificio Korta, Avd. Tolosa 72, E-20018 Donostia, Spain.

CORRELATED ELECTRON TRANSPORT IN MOLECULAR JUNCTIONS

K. S. Thygesen and A. Rubio

1 INTRODUCTION

The dimensions of conventional silicon based electronics devices will soon be so small that quantum effects, such as electron tunneling and energy quantization, will begin to influence and eventually limit the device functionality. On the other hand molecular electronics is based on the idea of constructing electronic devices from bottom up using organic molecules as basic building blocks and in this way integrate the quantum nature of the charge carriers directly in the design (Cuniberti *et al.* 2005 and Joachim *et al.* 2000). Over the last decade it has become possible to capture individual nanostructures between metal contacts and measure the electrical properties of the resulting junction. The types of nanostructures vary all the way from a single hydrogen molecule (Smit *et al.* 2002) over organic molecules (Reichert *et al.* 2002) to metallic chains of single atoms (Yanson *et al.* 1998) to carbon nanotubes suspended over several nanometers (Nygard *et al.* 2000) and inorganic nanowires and biochromophores (Cuniberti *et al.* 2005). The physics of these systems is highly non-classical showing intriguing phenomena such as quantized conductance, conductance oscillations, strong electron-phonon coupling, Kondo physics, and Coulomb blockade. For this reason a microscopic, i.e. quantum mechanical, understanding of nanoscale systems out of equilibrium is fundamental for the future development of molecular electronics.

The theoretical description of electron transport in molecules (we often use the term molecule to cover a general nanostructure) represents a central challenge in computational nanoscience. In principle, the problem involves an open quantum system of electrons interacting with each other and the surrounding nuclei under the influence of an external bias

voltage. Fortunately, due to the large difference in mass between electrons and nuclei, it is often a good approximation to regard the nuclei as classical charges fixed in their equilibrium positions – at least for sufficiently low temperature and bias voltage. This reduces the problem to interacting electrons moving through the static potential created by the frozen lattice of nuclei. Further simplification is obtained by replacing the electron-electron interactions by a meanfield potential as is done in Hartree-Fock (HF) and Kohn-Sham (KS) theory. Within such independent-particle approximations Landauer's formula (Landauer 1970) applies, giving the conductance as the (elastic) transmission probability for electrons at the Fermi level times the conductance unit $G_0 = 2e^2/h$. Landauer's formula and, in particular, its equivalent formulation in terms of nonequilibrium Green's functions (NEGF) (Meir and Wingreen 1992), has formed the basis for almost all calculations of quantum transport in nano-scale systems. First-principles calculations are usually based on the KS scheme of Density Functional Theory (DFT) with a local exchange-correlation functional (Taylor *et al.* 2001, Brandbyge *et al.* 2002). These DFT transport schemes have been successfully applied to systems characterized by strong coupling between the molecule and the electrodes (Thygesen and Jacobsen 2005, Garci-Suarez *et al.* 2005), but systematically overestimates the conductance of weakly coupled systems (Heurich *et al.* 2002, Quek *et al.* 2007). Recently, it has been shown that the use of self-interaction corrected exchange-correlation functionals improves the agreement with experiments for such systems (Toher *et al.* 2005). However, such functionals contain parameters which basically controls the size of the energy gap between highest occupied (HOMO) and lowest unoccupied (LUMO) molecular orbitals which questions the predictive power of such an approach.

Apart from the problems related to the position of molecular energy levels, there are a number of electronic effects originating from the two-body nature of the electron-electron interaction, which cannot – even in principle – be described within a single-particle picture. These include strong correlation effects like Kondo effects and Coulomb blockade (Goldhaber *et al.* 1998, Costi *et al.* 1994), renormalization of molecular levels by dynamic screening (Neaton *et al.* 2006, Kubatkin *et al.* 2003), and life-time reduction due to quasiparticle scattering (Thygesen 2008). As we shall see in this chapter, such dynamic correlation effects can have a dramatic influence on the electrical properties – in particular far from equilibrium.

In this chapter we describe how electronic correlation effects can be included in transport calculations using many-body perturbation theory within the Keldysh nonequilibrium Green's function formalism. Specifically, we use the so-called GW self-energy method (G denotes the Green's function and W is the screened interaction) which has been successfully applied to describe quasiparticle excitations in weakly correlated systems (Hybertsen and Louie 1986, Onida *et al.* 2002). To make the problem tractable, we limit the GW description to a central region containing the nanostructure of interest and part of the leads, while the (rest of the) metallic leads are treated at a mean-field level. The rationale behind this division is that the transport properties to a large extent are determined by the narrowest part of the conductor, i.e. the molecule, while the leads mainly serve as particle reservoirs (a proper inclusion of substrate polarization effects require that a sufficiently large part of the leads are included in the central region). The use of nonequilibrium many-body perturbation theory is only one out of several methods to include correlation effects in quantum transport. In another approach the density matrix is obtained from a many-body wave function and the

non-equilibrium boundary conditions are invoked by fixing the occupation numbers of left- and right going states (Delaney and Greer 2004). Exact diagonalization within the molecular subspace has been combined with rate equations to calculate tunneling currents to first order in the lead-molecule coupling strength (Hettler *et al.* 2003). The linear response conductance of jellium quantum point contacts has been addressed on the basis of the Kubo formula which in principle allows correlation effects to be incorporated through the response function (Bokes *et al.* 2007). The time-dependent version of density functional theory has also been used as framework for quantum transport (Stefanucci *et al.* 2007, Di Ventra and Todorov 2004). This scheme is particularly useful for simulating transients and high frequency ac-responses and can in principle include correlations via non-adiabatic exchange-correlation Kernels.

In section 2 we formulate the quantum transport problem and give a brief introduction to the nonequilibrium Green's function formalism. In section 3 we present the nonequilibrium GW equations and discuss the important concept of conserving approximations. In section 4.1 we obtain an expression for the current within the NEGF formalism which holds for interactions in the central region. It is demonstrated, both analytically and by numerical examples, that a self-consistent evaluation of the GW self-energy is fundamentally important for nonequilibrium transport as it – in contrast to the popular non self-consistent approach – ensures the validity of the continuity equation. In section 5, with the aim of identifying universal trends, we study a generic two-level model of a molecular junction. It is demonstrated how dynamic polarization effects renormalize the molecular levels, and a physical interpretation in terms of constrained total energy differences is provided. The application of a bias voltage is shown to enhance the dynamic polarization effects. Moreover, quasiparticle scattering becomes increasingly important at larger bias leading to a significant broadening of the molecular resonances. These effects, which are all beyond the single-particle approximation, have large impact on the calculated IV curve. In section 6 we combine the GW-transport scheme with DFT (for the leads) and a Wannier function basis set, and apply it to two prototypical junctions, namely a benzene molecule coupled to featureless leads and a hydrogen molecule between infinite Pt chains, and the results are analyzed using the knowledge obtained from the two-level model. It is found that non self-consistent G_0W_0 calculations depend crucially on the G_0 (whether it is the Hartree-Fock or Kohn-Sham Green's function). This together with its non conserving nature suggests that GW-transport calculations should be performed self-consistently.

This chapter is a summary of recent work by the authors on incorporating many-body correlation effects in quantum transport, see Thygesen and Rubio 2007, Thygesen and Rubio 2008, and Thygesen 2008.

2 FORMALISM

In this section we formulate the quantum transport problem and review the elements of the Keldysh Green's function theory needed for its solution. For more detailed introductions to the subject we refer to the books by Leeuwen *et al.* 2006 and Haug and Jauho 1998. To limit the technical details we specialize to the case of an orthogonal basis set and refer to Thygesen (2006) for a generalization to the non-orthogonal case.

2.1 Model

We consider a quantum conductor consisting of a central region (C) connected to left (L) and right (R) leads. For times $t < t_0$ the three regions are decoupled from each other, each being in thermal equilibrium with a common temperature and chemical potentials μ_L, μ_C, and μ_R, respectively (see Fig. 1). At $t = t_0$ the coupling between the three subsystems is switched on and a current starts to flow as the electrode with higher chemical potential discharges through the central region into the lead with lower chemical potential. Our aim is to calculate the steady state current which arises after the transient has died out. Notice that the duration of the steady state is determined by the size of the leads which we henceforth take to be infinite.

The single-particle state space of the electrons, $\mathcal{H}$, is spanned by the orthonormal basis set $\{\phi_i\}$. The orbitals ϕ_i are assumed to be localized such that $\mathcal{H}$ can be decomposed into a sum of orthogonal subspaces corresponding to the division of the system into leads and central region, i.e. $\mathcal{H} = \mathcal{H}_L + \mathcal{H}_C + \mathcal{H}_R$. We will use the notation $i \in \alpha$ to indicate that $\phi_i \in \mathcal{H}_\alpha$ for some $\alpha \in \{L, C, R\}$. The non-interacting part of the Hamiltonian of the *connected* system is written

$$\hat{h} = \sum_{\substack{i,j \in \\ L,C,R}} \sum_{\sigma=\uparrow\downarrow} h_{ij} c^\dagger_{i\sigma} c_{j\sigma} \tag{1}$$

where i, j run over all basis states of the system. For $\alpha, \beta \in \{L, C, R\}$, the operator $\hat{h}_{\alpha\beta}$ is obtained by restricting i to region α and j to region β in Eq. (1). Occasionally we shall write $\hat{h}_\alpha$ instead of $\hat{h}_{\alpha\alpha}$. We assume that there is no direct coupling between the two leads, i.e. $\hat{h}_{LR} = \hat{h}_{RL} = 0$ (this condition can always be fulfilled by increasing the size of the central region since the basis functions are localized). We introduce a special notation for the "diagonal" of $\hat{h}$,

$$\hat{h}_0 = \hat{h}_{LL} + \hat{h}_{CC} + \hat{h}_{RR}. \tag{2}$$

It is instructive to note that $\hat{h}_0$ does *not* describe the three regions in physical isolation from each other, but rather the contacted system without inter-region hopping. We allow for interactions between electrons inside the central region. The most general form of such a two-body interaction is,

$$\hat{V} = \sum_{\substack{ijkl \in C \\ \sigma\sigma'}} V_{ij,kl} c^\dagger_{i\sigma} c^\dagger_{j\sigma'} c_{l\sigma'} c_{k\sigma}. \tag{3}$$

The full Hamiltonian describing the system at time t can then be written

$$\hat{H}(t) = \begin{cases} \hat{H}_0 = \hat{h}_0 + \hat{V} & \text{for } t < t_0 \\ \hat{H} = \hat{h} + \hat{V} & \text{for } t > t_0 \end{cases} \tag{4}$$

Notice, that we use small letters for non-interacting quantities while the subscript 0 refers to uncoupled quantities. At this point we shall not be concerned about the actual value of the matrix elements h_{ij} and $V_{ij,kl}$ as this is unimportant for the general formalism discussed here.

For times $t < t_0$ each of the three subsystems are assumed to be in thermal equilibrium characterized by their equilibrium density matrices. For the left lead we have

$$\hat{\varrho}_L = \frac{1}{Z_L} \exp(-\beta(\hat{h}_L - \mu_L \hat{N}_L)) \tag{5}$$

with

$$Z_L = \mathrm{Tr}[\exp(-\beta(\hat{h}_L - \mu_L \hat{N}_L))]. \tag{6}$$

Here β is the inverse temperature and $\hat{N}_L = \sum_{\sigma, i\in L} c^\dagger_{i\sigma} c_{i\sigma}$ is the number operator of lead L. $\hat{\varrho}_R$ and Z_R are obtained by replacing L by R. For $\hat{\varrho}_C$ and Z_C we must add $\hat{V}$ to the Hamiltonian in the exponential to account for the correlations. The initial state of the whole system is given by

$$\hat{\varrho} = \hat{\varrho}_L \hat{\varrho}_C \hat{\varrho}_R. \tag{7}$$

If $\hat{V}$ is *not* included in $\hat{\varrho}_C$ we obtain the uncorrelated, or non-interacting, initial state $\hat{\varrho}_{ni}$. Because $\hat{H}_0$ ($\hat{h}_0$) describes the *contacted* system in the absence of inter-region hopping, $\hat{\varrho}$ ($\hat{\varrho}_{ni}$) do not describe the three regions in physical isolation. In other words the three regions are only decoupled at the *dynamic* level for times $t < t_0$.

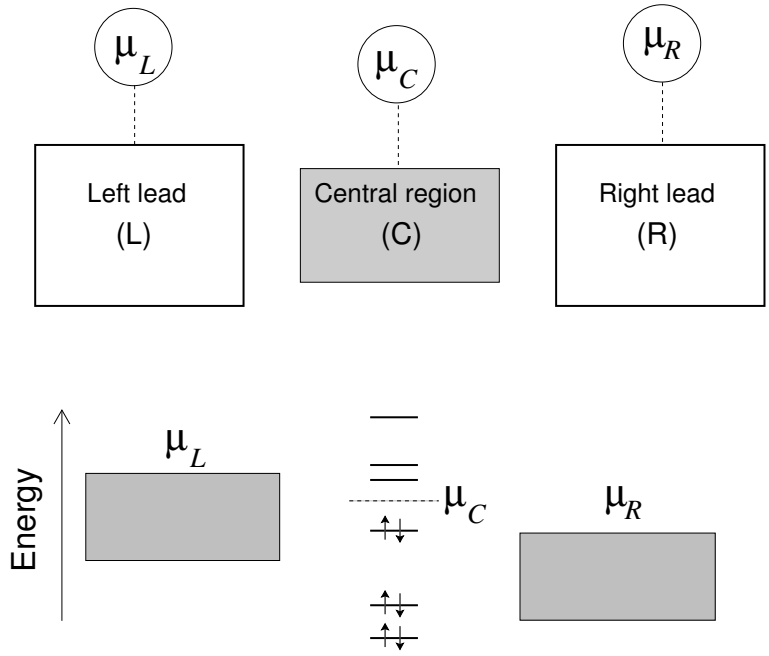

Figure 1: Before the coupling between the leads and central region is established, the three subsystems are in equilibrium with chemical potentials μ_L, μ_T, and μ_C, respectively. Reprinted with permission from Thygesen and Rubio, Phys. Rev. B **77**, 115333 (2008). Copyright 2008 by the American Physical Society.

2.2 Contour-ordered Green's function

To treat nonequilibrium problems it is useful to extend the time-propagation operator from the real time axis to the so-called Keldysh contour, $\mathcal{C}_I$, depicted in Fig. 2(a). The contour is defined in the complex plane and runs along the real axis from t_0 to infinity, then back to t_0 and vertically down to $t_0 - i\beta$. When τ and τ' denote points on the Keldysh contour, the generalized time-propagation operator is defined by

$$\hat{U}(\tau', \tau) = T e^{-i\int_\tau^{\tau'} \mathrm{d}\bar{\tau} \hat{H}(\bar{\tau})}, \tag{8}$$

where T orders a product of operators according to their time argument on the contour (later times further to the left). The integral is taken along $\mathcal{C}_I$. So far we have defined the Hamiltonian $\hat{H}(\tau)$ only for τ on the real axis. For Eq. (8) to make sense we must extend $\hat{H}(\tau)$ to the vertical branch of $\mathcal{C}_I$ which we will do in a moment. The contour-ordered single-particle GF relevant for our transport problem is defined by

$$G_{i\sigma,j\sigma'}(\tau,\tau') = -i\mathrm{Tr}\{\hat{\varrho}T[c_{H,i\sigma}(\tau)c^{\dagger}_{H,j\sigma'}(\tau')]\}, \tag{9}$$

where e.g. $c_{H,i\sigma}(\tau) = \hat{U}(t_0,\tau)c_{i\sigma}\hat{U}(\tau,t_0)$ and $\hat{\varrho}$ is the state of the system at time t_0. Notice that when evaluating $c_{H,i\sigma}(\tau)$ for τ on the real axis it does not matter whether τ is chosen on the upper or lower part of the contour. Notice also that when τ and τ' are both in the vertical branch, G is nothing but the Matsubara GF known from the equilibrium theory. For later reference we also note that a non-equilibrium GF is completely defined once (i) the Hamiltonian governing the dynamics and (ii) the initial state have been specified. Since the Hamiltonian contains no spin-flip processes the GF is diagonal in spin space, i.e. $G_{i\sigma,j\sigma'} = \delta_{\sigma\sigma'}G_{ij}$ and we therefore suppress the spin-dependence in the following.

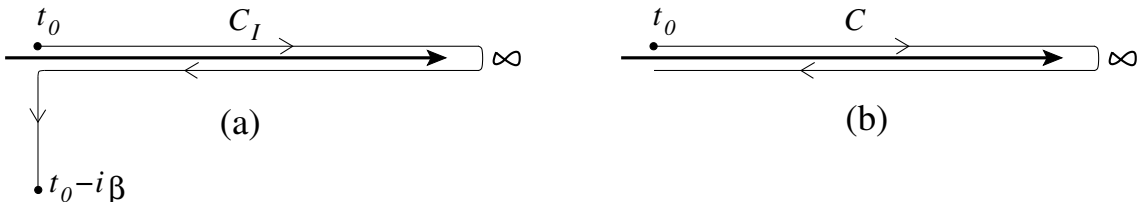

Figure 2: (a) The Keldysh contour $\mathcal{C}_I$. The dynamics of the system is governed by the Hamiltonian $\hat{H}(\tau)$ on the horizontal branch, while the initial state is defined by $\hat{H}(\tau)$ on the vertical branch. (b) The Keldysh contour $\mathcal{C}$, used when correlations in the initial state are neglected.

If we define $\hat{H}(\tau)$ along the vertical part of the contour to be

$$\hat{H}(\tau) = \sum_{\alpha=L,C,R}(\hat{h}_\alpha - \mu_\alpha\hat{N}_\alpha) + \hat{V}, \tag{10}$$

we see that $\hat{U}(t_0 - i\beta, t_0) = Z\hat{\varrho}$. We use this observation to write

$$G_{ij}(\tau,\tau') = -i\frac{\mathrm{Tr}\{T[e^{-i\int_{\mathcal{C}_I}\mathrm{d}\bar{\tau}\hat{H}(\bar{\tau})}c_i(\tau)c^{\dagger}_j(\tau')]\}}{\mathrm{Tr}\{Te^{-i\int_{\mathcal{C}_I}\mathrm{d}\bar{\tau}\hat{H}(\bar{\tau})}\}}. \tag{11}$$

Here the time-argument of $c_i(\tau)$ and $c^{\dagger}_j(\tau')$ only serves to identify their position in the contour-ordering, i.e. they are *not* in the Heisenberg picture. In order to obtain an expansion of $G_{ij}(\tau,\tau')$ in powers of $\hat{V}$, we switch to the interaction picture defined by the non-interacting Hamiltonian $\hat{h}(\tau) = \hat{H}(\tau) - \hat{V}$. In this picture we have

$$G_{ij}(\tau,\tau') = -i\frac{\mathrm{Tr}\{\hat{\varrho}_{ni}T[e^{-i\int_{\mathcal{C}_I}\mathrm{d}\bar{\tau}\hat{V}_h(\bar{\tau})}c_{h,i}(\tau)c^{\dagger}_{h,j}(\tau')]\}}{\mathrm{Tr}\{\varrho_{ni}Te^{-i\int_{\mathcal{C}_I}\mathrm{d}\bar{\tau}\hat{V}_h(\bar{\tau})}\}}, \tag{12}$$

where the time-dependence of the operators is governed by the evolution operator in Eq. (8) with $\hat{H}$ replaced by $\hat{h}$. The density matrix $\hat{\varrho}_{ni}$ is given by

$$\hat{\varrho}_{ni} = \frac{\exp(-\beta \sum_\alpha (\hat{h}_\alpha - \mu_\alpha \hat{N}_\alpha))}{\mathrm{Tr}\{\exp(-\beta \sum_\alpha (\hat{h}_\alpha - \mu_\alpha \hat{N}_\alpha))\}}, \tag{13}$$

which differs from $\hat{\varrho}$ in that it does not contain interactions in the central region. From the identity

$$Z\hat{\varrho} = Z_0 \hat{\varrho}_{ni} T e^{-i\int_{t_0}^{t_0-i\beta} \mathrm{d}\bar{\tau} \hat{V}_h(\bar{\tau})} \tag{14}$$

it is clear that the integration along the vertical branch of $\mathcal{C}_I$ in Eq. (12) accounts for the correlations in the initial state of region C. While it must be expected that the presence of initial correlations will influence the transient behavior of the current, it seems plausible that they will be washed out over time such that the steady state current will not depend on whether or not correlations are present in the initial state. In practice the neglect of initial correlations is a major simplification which allows us to work entirely on the real axis avoiding any reference to the imaginary time. For these reasons we shall neglect initial correlations in the rest of this paper. The GF can then be written

$$G_{ij}(\tau, \tau') = -i \frac{\mathrm{Tr}\{\hat{\varrho}_{ni} T[e^{-i\int_\mathcal{C} \mathrm{d}\bar{\tau} \hat{V}_h(\bar{\tau})} c_{h,i}(\tau) c^\dagger_{h,j}(\tau')]\}}{\mathrm{Tr}\{\hat{\varrho}_{ni} T e^{-i\int_\mathcal{C} \mathrm{d}\bar{\tau} \hat{V}_h(\bar{\tau})}\}}, \tag{15}$$

where the contour $\mathcal{C}$ is depicted in Fig. 2(b). Eq. (15) is the starting point for a systematic series expansion of G_{ij} in powers of $\hat{V}$. Since $\hat{\varrho}_{ni}$ is a mixed state of Slater determinants and the time-evolution is given by the non-interacting Hamiltonian, $\hat{h}$, Wick's theorem applies and leads to the standard Feynman rules with the exception that all time integrals are along the contour $\mathcal{C}$ and all Green's functions are contour-ordered. The Feynman diagrams should be constructed using the Green's function defined by $\hat{\varrho}_{ni}$ and $\hat{h}$,

$$g_{ij}(\tau, \tau') = -i\mathrm{Tr}\{\hat{\varrho}_{ni} T[c_{h,i}(\tau) c^\dagger_{h,j}(\tau')]\} \tag{16}$$

which describes the non-interacting electrons in the contacted system.

The diagrammatic expansion leads to the identification of a self-energy, Σ, as the sum of all irreducible diagrams with no external vertices. The GF is related to the self-energy and the non-interacting GF through Dyson's equation

$$G(\tau, \tau') = g(\tau, \tau') + \int_\mathcal{C} \mathrm{d}\tau_1 \mathrm{d}\tau_2 g(\tau, \tau_1) \Sigma(\tau_1, \tau_2) G(\tau_2, \tau'), \tag{17}$$

where matrix multiplication is implied. As we will see in Sec. 4.2, only the Green's function of the central region is needed for the calculation of the current, and we can therefore focus on the central-region submatrix of G. Since the interactions are limited to the central region, the self-energy matrix, Σ_{ij}, will be non-zero only when both $i, j \in C$, and it should therefore be safe to use the notation Σ instead of Σ_C. Restricting Eq. (17) to the central region we have

$$\begin{aligned} G_C(\tau, \tau') &= g_C(\tau, \tau') \\ &+ \int_\mathcal{C} \mathrm{d}\tau_1 \mathrm{d}\tau_2 g_C(\tau, \tau_1) \Sigma(\tau_1, \tau_2) G_C(\tau_2, \tau'). \end{aligned} \tag{18}$$

The free propagator, $g_C(\tau,\tau')$, is a non-equilibrium GF because $\hat{\varrho}_{ni}$ is not a stationary state of $\hat{h}$, i.e. $[\hat{\varrho}_{ni},\hat{h}]\neq 0$. It is, however, not difficult to show that g_C satisfies the following Dyson equation

$$g_C(\tau,\tau') = g_{0,C}(\tau,\tau') + \int_{\mathcal{C}} \mathrm{d}\tau_1 \mathrm{d}\tau_2 g_{0,C}(\tau,\tau_1) \\ [\Sigma_L(\tau_1,\tau_2)+\Sigma_R(\tau_1,\tau_2)] g_C(\tau_2,\tau'), \tag{19}$$

where g_0 is the *equilibrium* GF defined by $\hat{\varrho}_{ni}$ and $\hat{h}_0$. The coupling self-energy due to lead $\alpha = L,R$ is given by

$$\Sigma_\alpha(\tau,\tau') = h_{C\alpha} g_{0,\alpha}(\tau,\tau') h_{\alpha C}. \tag{20}$$

Notice the slight abuse of notation: Σ_α is *not* the $\alpha\alpha$ submatrix of Σ. In fact Σ_L and Σ_R are both matrices in the central region indices only. Combining Eqs. (18) and (19) we can write the Dyson equation for G_C,

$$\begin{aligned} G_C(\tau,\tau') &= g_{0,C}(\tau,\tau') \\ &+ \int_{\mathcal{C}} \mathrm{d}\tau_1 \mathrm{d}\tau_2 g_{0,C}(\tau,\tau_1)\Sigma_{tot}(\tau_1,\tau_2) G_C(\tau_2,\tau'), \end{aligned} \tag{21}$$

in terms of the equilibrium propagator of the non-interacting, uncoupled system, g_0, and the total self-energy

$$\Sigma_{tot} = \Sigma + \Sigma_L + \Sigma_R. \tag{22}$$

The total self-energy describes the combined effect of the interactions and the coupling to the leads.

2.3 Real-time Green's functions

In order to evaluate expectation values of single-particle observables we need the real-time correlation functions. We work with two correlation functions, also called the lesser and greater GFs, defined as

$$G^<_{ij}(t,t') = i\mathrm{Tr}\{\hat{\varrho}_{ni} c^\dagger_{H,j}(t') c_{H,i}(t)\} \tag{23}$$

$$G^>_{ij}(t,t') = -i\mathrm{Tr}\{\hat{\varrho}_{ni} c_{H,i}(t) c^\dagger_{H,j}(t')\}. \tag{24}$$

Again, the use of $\hat{\varrho}_{ni}$ instead of $\hat{\varrho}$ amounts to neglecting initial correlations. Two other important real-time GFs are the retarded and advanced GFs defined by

$$G^r_{ij}(t,t') = \theta(t-t')(G^>_{ij}(t,t') - G^<_{ij}(t,t')) \tag{25}$$

$$G^a_{ij}(t,t') = \theta(t'-t)(G^<_{ij}(t,t') - G^>_{ij}(t,t')). \tag{26}$$

The four GFs are related through

$$G^> - G^< = G^r - G^a. \tag{27}$$

The lesser and greater GFs are just special cases of the contour-ordered GF. For example $G^<(t,t') = G(\tau,\tau')$ when $\tau = t$ is on the upper branch of $\mathcal{C}$ and $\tau' = t'$ is on the lower branch. This can be used to derive a set of rules, sometimes referred to as the Langreth rules, for converting expressions involving contour-ordered quantities into equivalent expressions involving

real-time quantities. We shall not list the conversion rules here, but refer to Haug and Jauho 1998 (no initial correlations) and Leeuwen *et al.* 2006 (including initial correlations). The usual procedure in non-equilibrium is then to derive the relevant equations on the contour using the standard diagrammatic techniques, and subsequently converting these equations to real time by means of the Langreth rules. An example of this procedure is given in Sec. 3.2 where the non-equilibrium GW equations are derived.

2.3.1 Equilibrium

In equilibrium, the real-time GFs depend only on the time difference $t'-t$. Fourier transforming with respect to this time difference then brings out the spectral properties of the system. In particular the spectral function

$$A(\omega) = i[G^r(\omega) - G^a(\omega)] = i[G^>(\omega) - G^<(\omega)] \tag{28}$$

shows peaks at the *quasiparticle* energies of the system, i.e. at the energies $E_n(N+1)-E_m(N)$ and $E_m(N) - E_n(N-1)$, where n, m denote energy levels and N the number of electrons. We thus see that the single-particle GF carries information about the electron addition- and removal energies. Clearly these are the types of excitations which are relevant in a transport situation where electrons are continuously added to and removed from the central region. In section 5.2 we discuss how many-body polarization effects renormalize the spectral function of a molecule adsorbed at a metal surface. In equilibrium we furthermore have the important fluctuation-dissipation theorem which relates the correlation functions to the spectral function and the Fermi-Dirac distribution function, f,

$$G^<(\omega) = if(\omega)A(\omega) \tag{29}$$
$$G^>(\omega) = -i(1-f(\omega))A(\omega). \tag{30}$$

The fluctuation-dissipation theorem follows from the Lehman representation which no longer holds out of equilibrium, and as a consequence one has to work explicitly with the correlation functions in non-equilibrium situations.

2.3.2 Non-equilibrium steady state

We shall make the plausible assumption that in steady state, all the real-time GFs depend only on the time-difference $t'-t$. Moreover, we take the limit $t_0 \to -\infty$. This will allow us to use the Fourier transform to turn convolutions in real time into products in frequency space. Applying the Langreth conversion rules to the Dyson equation (21), and Fourier transforming with respect to $t'-t$ then leads to the following expression for the retarded GF of the central region

$$G^r_C(\omega) = g^r_{0,C}(\omega) + g^r_{0,C}(\omega)\Sigma^r_{tot}(\omega)G^r_C(\omega). \tag{31}$$

This equation can be inverted to yield the closed form

$$G^r_C(\omega) = [(\omega + i\eta)I_C - h_C - \Sigma^r_L(\omega) - \Sigma^r_R(\omega) - \Sigma^r(\omega)]^{-1}. \tag{32}$$

The equation for G^a is obtained by replacing r by a and η by $-\eta$ or, alternatively, from

$$G^a_C(\omega) = [G^r_C(\omega)]^\dagger, \tag{33}$$

which follows from the assumption that the GFs depend on time differences only. For the correlation functions the conversion rules leads to the expression

$$G_C^{</>}(\omega) = G_C^r(\omega)\Sigma_{tot}^{</>}(\omega)G_C^a(\omega) + \Delta^{</>}(\omega) \tag{34}$$

where

$$\Delta^{</>}(\omega) = [I_C + G_C^r(\omega)\Sigma_{tot}^r(\omega)]g_{0,C}^{</>}(\omega)[I_C + \Sigma_{tot}^a(\omega)G_C^a(\omega)]. \tag{35}$$

Using that $\Sigma_{tot}^{r/a} = (g_{0,C}^{r/a})^{-1} - (G_C^{r/a})^{-1}$ together with the equilibrium relations $g_{0,C}^< = -f(\omega - \mu_C)[g_{0,C}^r - g_{0,C}^a]$ and $g_{0,C}^> = -(f(\omega-\mu_C)-1)[g_{0,C}^r - g_{0,C}^a]$, we find that

$$\Delta^<(\omega) = 2i\eta f(\omega-\mu_C)G_C^r(\omega)G_C^a(\omega) \tag{36}$$

$$\Delta^>(\omega) = 2i\eta[f(\omega-\mu_C)-1]G_C^r(\omega)G_C^a(\omega). \tag{37}$$

If the product G^rG^a is independent of η we can conclude that $\Delta \to 0$ in the relevant limit of small η. It can in fact be shown that Δ always vanishes for interacting electrons while for non-interacting electrons Δ vanishes only when there are no bound states (Thygesen and Rubio 2008).

2.3.3 Non-interacting electrons and lead self-energy

In the special case of non-interacting electrons, the retarded and advanced GFs are independent of the initial state of the system, i.e. of the $\hat{\varrho}$ entering the GF. Moreover, if the dynamics is governed by a time-independent Hamiltonian, g^r and g^a depend only on the time difference $t'-t$ (even if the initial state is not a stationary state). In this case the Fourier transform of the retarded and advanced GFs with respect to $t'-t$ equals the resolvent of the Hamiltonian matrix h,

$$g^{r/a}(\omega) = [(\omega \pm i\eta)I - h]^{-1}, \tag{38}$$

where I is the identity matrix and η is a positive infinitesimal. In our transport problem, the block-diagonal structure of h_0 allows us to obtain the non-interacting GF of the uncoupled system by inverting each block separately,

$$g_{0,\alpha}^{r/a}(\omega) = [(\omega \pm i\eta)I - h_\alpha]^{-1} \tag{39}$$

for $\alpha \in \{L, C, R\}$. Now it is in fact easy to show that the central region component of $g^{r/a}$ satisfies

$$g_C^{r/a}(\omega) = [(\omega \pm i\eta)I - h_C - \Sigma_L^{r/a}(\omega) - \Sigma_R^{r/a}(\omega)]^{-1}, \tag{40}$$

with the retarded/advanced coupling self-energies given by

$$\Sigma_\alpha^{r/a}(\omega) = h_{C\alpha}g_{0,\alpha}^{r/a}(\omega)h_{\alpha C}. \tag{41}$$

Eqs. (40) and (41) give the retarded and advanced components of Eqs. (19) and (20), respectively. Notice that $\Sigma_\alpha^{r/a}$ depends on the applied bias voltage through $g_{0,\alpha}$ because the self-consistent field in the leads follow the chemical potential to ensure charge neutrality as sketched in the lower panel of Fig. 1. Assuming a symmetrically applied bias ($\mu_{L/R} = \varepsilon_F \pm V/2$) we have

$$\Sigma_L^{r/a}(V;\omega) = \Sigma_L^{r/a}(0;\omega - V/2), \tag{42}$$

with a similar relation for Σ_R. Since g_0 is an equilibrium GF its lesser and greater components, and thus also $\Sigma_\alpha^{</>}$, follow from the fluctuation-dissipation theorem. In contrast, the correlation functions derived from g, which is a non-equilibrium function, must be calculated using the Keldysh equation (34).

3 MANY-BODY SELF-ENERGY

In this section we discuss two specific approximations to the many-body self-energy Σ introduced in Eq. (17), namely the *GW* and second Born (2B) approximations. Strictly speaking the Σ of Eq. (17) contains the full effect of the interactions whereas the *GW* and 2B self-energies only describe exchange and correlation, i.e. they do not include the Hartree potential. The *GW* self-energy is obtained by summing an infinite set of Feynman diagrams – one diagram at each order of the interaction – while the 2B approximation is exact to second order in the interaction (if performed self-consistently). In section 3.1 we introduce an effective interaction which leads to a particularly simple form of the self-energy equations and at the same time provides a means for reducing self-interaction errors in higher order diagrammatic expansions. In sections 3.2 and 3.3 we discuss the nonequilibrium *GW* and 2B equations using the effective interaction.

3.1 Effective interaction

The direct use of the full interaction Eq. (3) in a diagrammatic expansion is problematic as it introduces frequency dependent, four-index quantities, which quickly becomes difficult to store and handle numerically. For this reason we consider instead the effective interaction defined by

$$\hat{V}_{\text{eff}} = \sum_{ij,\sigma\sigma'} \tilde{V}_{i\sigma,j\sigma'} c^\dagger_{i\sigma} c^\dagger_{j\sigma'} c_{j\sigma'} c_{i\sigma}, \tag{43}$$

where

$$\tilde{V}_{i\sigma,j\sigma'} = V_{ij,ij} - \delta_{\sigma\sigma'} V_{ij,ji}. \tag{44}$$

This expression follows by restricting the sum in the full interaction Eq. (3) to terms of the form $V_{ij,ij} c^\dagger_{i\sigma} c^\dagger_{j\sigma'} c_{j\sigma'} c_{i\sigma}$ and $V_{ij,ji} c^\dagger_{i\sigma} c^\dagger_{j\sigma} c_{j\sigma} c_{i\sigma}$.

The effective interaction is local in orbital space, i.e. it is a two-point function instead of a four-point function and thus resembles the real-space representation. Note, however, that in contrast to the real-space representation $\tilde{V}_{i\sigma,j\sigma'}$ is spin-dependent. In particular the self-interactions, $\tilde{V}_{i\sigma,i\sigma}$, are zero by construction and consequently self-interaction (in the orbital basis) is avoided to all orders in a perturbation expansion in powers of $\tilde{V}$. Since the off-diagonal elements ($i \neq j$) of the exchange integrals $V_{ij,ji}$ are small for localized basis functions, the main effect of the second term in Eq. (44) is to cancel the self-interaction in the first term.

It is not straightforward to anticipate the quality of a many-body calculation based on the effective interaction (43) as compared to the full interaction (3). Clearly, if we include all Feynman diagrams in Σ, we obtain the exact result when the full interaction (3) is used, while the use of the effective interaction (43) would yield an approximate result. The quality of this approximate result would then depend on the basis set, becoming better the more localized the basis functions and equal to the exact result in the limit of completely localized delta functions where only the direct Coulomb integrals $V_{ij,ij}$ will be non-zero. However, when only a subset of all diagrams are included in Σ the situation is different: In the *GW* approximation for instance, only one diagram per order (in $\hat{V}$) is included, and thus cancellation of self-interaction does not occur when the full interaction is used. On the other hand the effective

interaction (44) is self-interaction free (in the orbital basis) by construction. The situation can be understood by considering the lowest order case. There are only two first order diagrams – the Hartree and exchange diagrams – and each cancel the self-interaction in the other. More generally, the presence of self-interaction in an incomplete perturbation expansion can be seen as a violation of identities of the form $\langle\cdot|c^\dagger_{k\sigma'}\cdots c_{i\sigma}c_{i\sigma}\cdots c_{j\sigma''}|\cdot\rangle = 0$, when not all Wick contractions are evaluated. Such expectation values will correctly vanish when the effective interaction is used because the prefactor of the $c_{i\sigma}c_{i\sigma}$ operator, $\tilde{V}_{i\sigma,i\sigma}$, is zero. The effect of self-interaction errors in (non-self consistent) GW calculations was recently studied for a hydrogen atom (Nelson *et al.* 2007). For a quantitative estimate of the quality of GW calculations based on $\hat{V}_{\text{eff}}$ we refer to Thygesen and Rubio 2008.

3.2 Non-equilibrium GW self-energy

It is useful to split the full many-body self-energy into its Hartree and exchange-correlation parts

$$\Sigma(\tau,\tau') = \Sigma_h(\tau,\tau') + \Sigma_{xc}(\tau,\tau'). \tag{45}$$

The Hartree term is local in time and can be written $\Sigma_h(\tau,\tau') = \Sigma_h(\tau)\delta_{\mathcal{C}}(\tau,\tau')$ where $\delta_{\mathcal{C}}$ is a delta function on the Keldysh contour. The xc- self-energy is nonlocal in time and contains all the complicated many-body effects. In the GW approximation the xc- self-energy is written as a product of the Green's function, G, and the screened interaction, W. Usually W is calculated in the random-phase approximation (RPA), and it has been found that improving W beyond RPA has little effect on the resulting GW self-energy (Verdozzi *et al.* 1995).

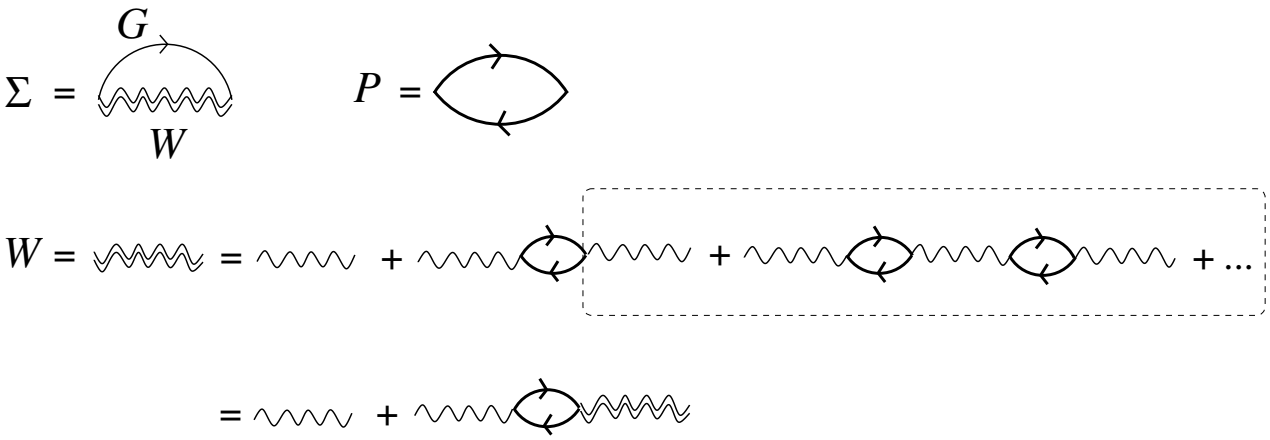

Figure 3: Feynman diagrams for the GW self-energy in terms of the Green's function (G), the screened interaction (W), and the polarization bubble (P). All quantities are functions of two Keldysh times, and two basis function indices. Integration/summation over internal times/indices is implied.

With the effective interaction (43) the screened interaction, W, and the polarization function, P, are reduced from four- to two-index functions. For notational simplicity we absorb the spin index into the orbital index, i.e. $(i\sigma) \to i$ (but we do not neglect it). The expression

for the contour-ordered GW self-energy in terms of contour-ordered quantities then read

$$\Sigma_{GW,ij}(\tau,\tau') = iG_{ij}(\tau,\tau'^{+})W_{ij}(\tau,\tau') \quad (46)$$

$$W_{ij}(\tau,\tau') = \tilde{V}_{ij}\delta_{\mathcal{C}}(\tau,\tau') + \sum_{kl}\int_{\mathcal{C}} \mathrm{d}\tau_1 \tilde{V}_{ik}P_{kl}(\tau,\tau_1)W_{lj}(\tau_1,\tau') \quad (47)$$

$$P_{ij}(\tau,\tau') = -iG_{ij}(\tau,\tau')G_{ji}(\tau',\tau). \quad (48)$$

It is important to notice that in contrast to the conventional real-space representation of the GW self-energy, the spin-dependence cannot be neglected when the effective interaction is used. The reason for this is that $\tilde{V}$ is spin-dependent and consequently the spin off-diagonal elements of W will influence the spin-diagonal elements of G, Σ, and P. A diagrammatic representation of the GW approximation is shown in Fig. 4. As they stand, equations (46)-(48) involve quantities of the whole system (leads and central region). However, since $\tilde{V}_{ij}$ is non-zero only when $i, j \in C$, it follows from Eq. (47), that W and hence Σ also have this structure. Consequently, the subscript C can be directly attached to each quantity in Eqs. (46)-(48), however, for the sake of generality and notational simplicity we shall not do so at this point. It is, however, important to realize that the GF appearing in the GW equations includes the self-energy due to the leads.

Using the Langreth conversion rules the retarded and lesser GW self-energies become (on the time axis),

$$\Sigma^{r}_{GW,ij}(t) = iG^{r}_{ij}(t)W^{>}_{ij}(t) + iG^{<}_{ij}(t)W^{r}_{ij}(t) \quad (49)$$

$$\Sigma^{</>}_{GW,ij}(t) = iG^{</>}_{ij}(t)W^{</>}_{ij}(t), \quad (50)$$

where we have used the variable t instead of the time difference $t' - t$. For the screened interaction we obtain (in frequency space),

$$W^{r}(\omega) = \tilde{V}[I - P^{r}(\omega)\tilde{V}]^{-1} \quad (51)$$

$$W^{</>}(\omega) = W^{r}(\omega)P^{</>}(\omega)W^{a}(\omega). \quad (52)$$

where all quantities are matrices in the indices i, σ and matrix multiplication is implied. Notice that the spin off-diagonal part of $\tilde{V}$ will affect the spin-diagonal part of W^r through the matrix inversion. Finally, the real-time components of the irreducible polarization become

$$P^{r}_{ij}(t) = -iG^{r}_{ij}(t)G^{<}_{ji}(-t) - iG^{<}_{ij}(t)G^{a}_{ji}(-t) \quad (53)$$

$$P^{</>}_{ij}(t) = -iG^{</>}_{ij}(t)G^{>/<}_{ji}(-t). \quad (54)$$

From their definitions it is clear that both the polarization and the screened interaction obey the relations $P^{a}_{ij}(\omega) = P^{r}_{ji}(-\omega)$ and $W^{a}_{ij}(\omega) = W^{r}_{ji}(-\omega)$, while for the self-energy and GFs we have $\Sigma^{a}_{GW}(\omega) = \Sigma^{r}_{GW}(\omega)^{\dagger}$ and $G^{a}(\omega) = G^{r}(\omega)^{\dagger}$. In addition all quantities fullfill the general identity $X^{>} - X^{<} = X^{r} - X^{a}$. We mention that the nonequilibrium GW approximation has previously been used to study band-gap renormalization in excited GaAs (Spataru *et al.* 2004).

In deriving Eqs. (51,52) we have made use of the conversion rules $\delta^{</>}_{\mathcal{C}}(t,t') = 0$ and $\delta^{r/a}_{\mathcal{C}}(t,t') = \delta(t-t')$. With these definitions the applicability of the Langreth rules can be

extended to functions containing delta functions on the contour. Notice, however, that with these definitions relation (25) does not hold for the delta function. The reason why the delta function requires a separate treatment is that the standard Langreth rules are derived under the assumption that all functions on the contour are well behaved, e.g. not containing delta functions. We stress that no spin symmetry has been assumed in the above GW equations. Indeed by reintroducing the spin index, i.e. $i \to (i\sigma)$ and $j \to (j\sigma')$, it is clear that spin-polarized calculations can be performed by treating $G_{\uparrow\uparrow}$ and $G_{\downarrow\downarrow}$ independently.

Within the GW approximation the full interaction self-energy is given by

$$\Sigma(\tau, \tau') = \Sigma_h(\tau, \tau') + \Sigma_{GW}(\tau, \tau'), \tag{55}$$

where the GW self-energy can be further split into an static exchange and a dynamic correlation part,

$$\Sigma_{GW}(\tau, \tau') = \Sigma_x \delta_{\mathcal{C}}(\tau, \tau') + \Sigma_{\rm corr}(\tau, \tau'). \tag{56}$$

Due to the static nature of Σ_h and Σ_x we have

$$\Sigma_h^{</>} = \Sigma_x^{</>} = 0. \tag{57}$$

The retarded components of the Hartree and exchange self-energies become constant in frequency space, and we have (note that for Σ_h and Σ_x we do *not* use the effective interaction (43))

$$\Sigma^r_{h,ij} = -i \sum_{kl} G^<_{kl}(t=0) V_{ik,jl} \tag{58}$$

$$\Sigma^r_{x,ij} = i \sum_{kl} G^<_{kl}(t=0) V_{ik,lj}. \tag{59}$$

Due to (57), it is clear that Eq. (50) yields the lesser/greater components of $\Sigma_{\rm corr}$. Since $\Sigma_{\rm corr}(\tau, \tau')$ does not contain delta functions its retarded component can be obtained from the relation,

$$\Sigma^r_{\rm corr}(t) = \theta(-t)[\Sigma^>_{GW}(t) - \Sigma^<_{GW}(t)]. \tag{60}$$

The separate calculation of Σ^r_x and $\Sigma^r_{\rm corr}$ from Eqs. (59),(60) as opposed to calculating their sum directly from Eq. (49), has two advantages: (i) It allows us to treat Σ_x, which is the dominant contribution to Σ_{GW}, at a higher level of accuracy than $\Sigma_{\rm corr}$. (ii) We avoid numerical operations involving G^r and W^r in the time domain. For more detailed discussions of these points see appendices A and E of Thygesen and Rubio 2008.

3.3 Non-equilibrium second Born approximation

When screening and/or strong correlation effects are less important, as e.g. in the case of small, isolated molecules, the higher-order terms of the GW approximation are small and it is more important to include all second order diagrams (Stan *et al.* 2006). The full second order approximation, often referred to as the second Born approximation (2B), is shown diagrammatically in Fig. 4. As we will use the 2B for comparison with the GW results we state the relevant expressions here for completeness.

On the contour the 2B self-energy reads (with the effective interaction (43))

$$\begin{aligned}\Sigma_{2B,ij}(\tau,\tau') &= \sum_{kl} G_{ij}(\tau,\tau')G_{kl}(\tau,\tau')G_{lk}(\tau',\tau)\tilde{V}_{ik}\tilde{V}_{jl} \\ &- \sum_{kl} G_{ik}(\tau,\tau')G_{kl}(\tau',\tau)G_{lj}(\tau,\tau')\tilde{V}_{il}\tilde{V}_{jk}\end{aligned} \tag{61}$$

Notice that the first term in Σ_{2B} is simply the second order term of the GW self-energy. From Eq. (61) it is easy to obtain the lesser/greater self-energies,

$$\begin{aligned}\Sigma^{</>}_{2B,ij}(t) &= \sum_{kl} G^{</>}_{ij}(t)G^{</>}_{kl}(t)G^{>/<}_{lk}(-t)\tilde{V}_{ik}\tilde{V}_{jl} \\ &- \sum_{kl} G^{</>}_{ik}(t)G^{>/<}_{kl}(-t)G^{</>}_{lj}(t)\tilde{V}_{il}\tilde{V}_{jk},\end{aligned}$$

where t has been used instead of the time difference $t - t'$. Since these second order contributions do not contain delta functions of the time variable, we can obtain the retarded self-energy directly from the Kramers-Kronig relation

$$\Sigma^r_{2B}(t) = \theta(-t)[\Sigma^>_{2B}(t) - \Sigma^<_{2B}(t)]. \tag{62}$$

4 CURRENT

As mentioned earlier, the current flowing between the electrodes can be calculated from the Green's function of the central region. After a short introduction to the concept of conserving approximations in section 4.1, we present the relevant formulas for evaluating the current under non-equilibrium conditions. In section 4.3 we then derive a condition on the interaction self-energy which ensures charge conservation in the sense that the current is the same at the left and right interface between the central region and the leads. Finally, in section 4.4 we show that this condition is always fulfilled for the so-called conserving, or Φ-derivable, self-energies.

4.1 Conserving approximations

Once a self-energy has been obtained the GF follows from the Dyson and Keldysh equations (32),(34). Any single-particle observable, such as the current or the density, can then be calculated from the GF. An important question is then whether the calculated quantities obey the fundamental conservation laws like charge- and energy conservation. In the context of modeling electron transport, the condition for charge conservation as expressed by the continuity equation

$$\frac{\mathrm{d}}{\mathrm{d}t}n(\mathbf{r},t) = -\nabla\cdot\mathbf{j}(\mathbf{r},t) \tag{63}$$

is obviously of particular interest.

Baym and Kadanoff (Baym and Kadanoff 1961, Baym 1962) showed that there exists a deep connection between the self-energy and the validity of the conservation laws. Precisely, any self-energy which can be written as a functional derivative, $\Sigma[G] = \delta\Phi[G]/\delta G$, where

$\Phi[G]$ belongs to a certain class of functionals of G, produces a GF which automatically fulfills the basic conservation laws. A self-energy which can be obtained in this way is called Φ-derivable. Since a Φ-derivable self-energy depends on G, the Dyson equation must be solved self-consistently. The exact $\Phi[G]$ can be obtained by summing over all skeleton diagrams constructed using the full G as propagator. By a skeleton diagram we mean a closed diagram, i.e. no external vertices, containing no self-energy insertions. Practical approximations are then obtained by including only a subset of skeleton diagrams. Two examples of such approximations are provided by the GW and second Born Φ-functionals and associated self-energies which are illustrated in Fig. 4. Another example is provided by the Hartree-Fock approximation. Solving the Dyson equation self-consistently with one of these self-energies thus defines a conserving approximation in the sense of Baym.

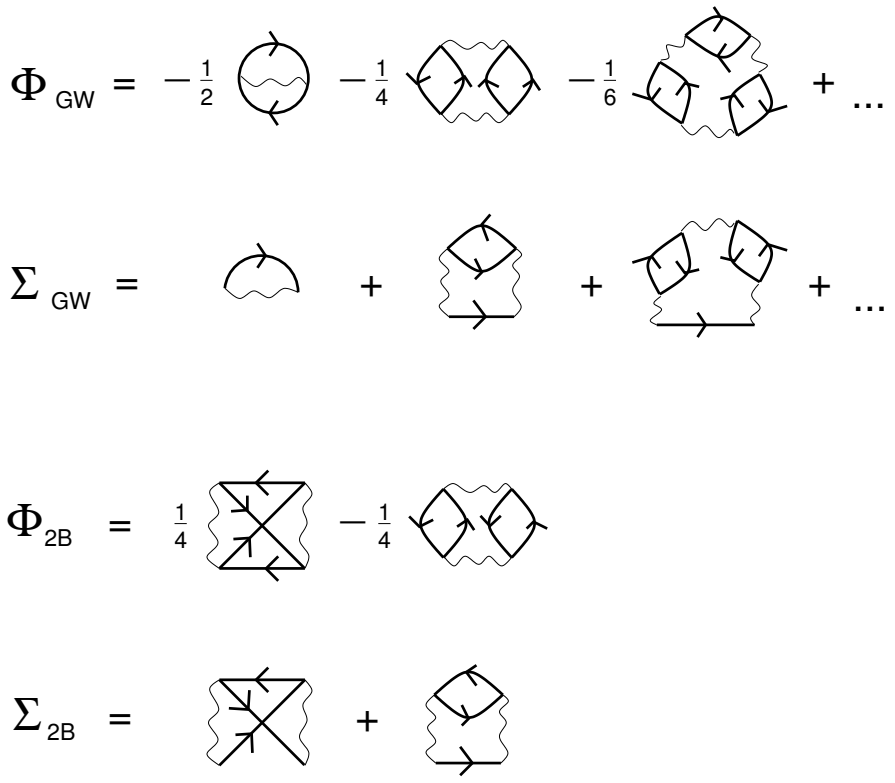

Figure 4: The GW and second Born self-energies, Σ_{GW} and Σ_{2B}, can be obtained as functional derivatives of their respective Φ-functionals, $\Phi_{GW}[G]$ and $\Phi_{2B}[G]$. Straight lines represent the full Green's function, G, i.e. the Green's function in the presence of coupling to the leads and interactions. Wiggly lines represent the interactions. Reprinted with permission from Thygesen and Rubio, Phys. Rev. B **77**, 115333 (2008). Copyright 2008 by the American Physical Society.

The validity of the conservation laws for Φ-derivable self-energies follows from the invariance of Φ under certain transformations of the Green's function. For example it follows from the closed diagramatic structure of Φ that the transformation

$$G(\mathbf{r}\tau, \mathbf{r}'\tau') \rightarrow e^{i\Lambda(\mathbf{r}\tau)} G(\mathbf{r}\tau, \mathbf{r}'\tau') e^{-i\Lambda(\mathbf{r}'\tau')}, \tag{64}$$

where Λ is any scalar function, leaves $\Phi[G]$ unchanged. Using the compact notation $(\mathbf{r}_1, \tau_1) = 1$, the change in Φ when the GF is changed by δG can be written as $\delta\Phi = \int \mathrm{d}1\mathrm{d}2\Sigma(1,2)\delta G(2,1^+) = 0$, where we have used that $\Sigma = \delta\Phi[G]/\delta G$. To first order in Λ we then have

$$\begin{aligned}\delta\Phi &= i\int \mathrm{d}1\mathrm{d}2\Sigma(1,2)[\Lambda(2)-\Lambda(1)]G(2,1^+)\\ &= i\int \mathrm{d}1\mathrm{d}2[\Sigma(1,2)G(2,1^+)-G(1,2^+)\Sigma(2,1)]\Lambda(1).\end{aligned}$$

Since this hold for all Λ (by a scaling argument) we conclude that

$$\int \mathrm{d}2[\Sigma(1,2)G(2,1^+)-G(1,2^+)\Sigma(2,1)] = 0. \tag{65}$$

This condition ensures the validity of the continuity equation (on the contour) at any point in space. In the following sections we derive and discuss this result in the framework of the transport model introduced in Section 2.

4.2 Current formula

When the coupling between the leads and the central region is established, a current will start to flow. The particle current from lead α into the central region is given by the time derivative of the number operator of lead α (Meir and Wingreen 1992),

$$\begin{aligned}I_\alpha(t) &= -i\langle[\hat{H},\hat{N}_\alpha](t)\rangle\\ &= i\sum_{\substack{i\in\alpha\\ n\in C}} G^<_{ni}(t,t)h_{in} - h_{ni}G^<_{in}(t,t).\end{aligned} \tag{66}$$

A simple diagrammatic argument shows that ($i\in\alpha$, $n\in C$)

$$\begin{aligned}G_{ni}(\tau,\tau') &= \sum_{\substack{j\in\alpha\\ m\in C}}\int_{\mathcal{C}}\mathrm{d}\tau_1 G_{nm}(\tau,\tau_1)h_{mj}g_{0,ji}(\tau_1,\tau')\\ G_{in}(\tau,\tau') &= \sum_{\substack{j\in\alpha\\ m\in C}}\int_{\mathcal{C}}\mathrm{d}\tau_1 g_{0,ij}(\tau,\tau_1)h_{jm}G_{mn}(\tau_1,\tau').\end{aligned}$$

Using Eq (20) we notice that Eq. (66) can be written as $i\mathrm{Tr}[A^<(t,t)]$ when A is defined as in Eq. (92) with $B = G_C$ and $C = \Sigma_\alpha$. From the general result (93) it then follows that

$$I_\alpha = \int \frac{\mathrm{d}\omega}{2\pi}\mathrm{Tr}\big[\Sigma^<_\alpha(\omega)G^>_C(\omega) - \Sigma^>_\alpha(\omega)G^<_C(\omega)\big], \tag{67}$$

where matrix multiplication is implied. By writing $I = (I_L - I_R)/2$ we obtain an expression which is symmetric in the L, R indices,

$$I = \frac{i}{4\pi}\int \mathrm{Tr}[(\Gamma_L-\Gamma_R)G^<_C + (f_L\Gamma_L - f_R\Gamma_R)(G^r_C - G^a_C)]\mathrm{d}\omega \tag{68}$$

where we have suppressed the ω dependence and introduced the coupling strength of lead α, $\Gamma_\alpha = i[\Sigma^r_\alpha - \Sigma^a_\alpha]$. We notice that when interactions are present, the integrals in Eqs. (68) and (67) will have contributions outside the bias window, $\mu_L < \omega < \mu_R$, because the conduction electrons can gain or lose energy by interacting with other electrons in the central region.

4.3 Charge conservation

Due to charge conservation in the steady state we expect that $I_L = -I_R = I$, i.e. the current flowing from the left lead to the molecule is the negative of the current flowing from the right lead to the molecule. Below we derive a condition for this specific form of particle conservation.

From Eq. (67) the difference between the currents at the left and right interface, $\Delta I = I_L + I_R$, is given by

$$\Delta I = \int \frac{\mathrm{d}\omega}{2\pi} \mathrm{Tr}\big[(\Sigma_L^< + \Sigma_R^<)G_C^> - (\Sigma_L^> + \Sigma_R^>)G_C^<\big] \tag{69}$$

To obtain a condition for $\Delta I = 0$ in terms of Σ we start by proving the general identity

$$\int \frac{\mathrm{d}\omega}{2\pi} \mathrm{Tr}\big[\Sigma_{tot}^<(\omega)G_C^>(\omega) - \Sigma_{tot}^>(\omega)G_C^<(\omega)\big] = 0. \tag{70}$$

To prove this, we insert $G^{</>} = G_C^r \Sigma_{tot}^{</>} G_C^a + \Delta^{</>}$ (from Eq. (34)) in the left hand side of Eq. (70). This results in two terms involving $G^r \Sigma_{tot}^{</>} G^a$ and two terms involving $\Delta^{</>}$. The first two terms contribute by

$$\int \frac{\mathrm{d}\omega}{2\pi} \mathrm{Tr}\big[\Sigma_{tot}^< G^r \Sigma_{tot}^> G^a - \Sigma_{tot}^> G^r \Sigma_{tot}^< G^a\big]. \tag{71}$$

Inserting $\Sigma_{tot}^> = \Sigma_{tot}^< + (G^a)^{-1} - (G^r)^{-1}$ (we use that $(G^a)^{-1} - (G^r)^{-1} = \Sigma_{tot}^r - \Sigma_{tot}^a = \Sigma_{tot}^> - \Sigma_{tot}^<$) in this expression and using the cyclic invariance of the trace, it is straightforward to show that Eq. (71) vanishes. The two terms involving $\Delta^{</>}$ contribute to the left hand side of Eq. (70) by

$$\int \frac{\mathrm{d}\omega}{2\pi} \mathrm{Tr}\big[\Sigma_{tot}^<(\omega)\Delta^>(\omega) - \Sigma_{tot}^>(\omega)\Delta^<(\omega)\big]. \tag{72}$$

As mentioned in section 2.3.2, $\Delta^<$ and $\Delta^>$ are always zero when interactions are present. In the case of non-interacting electrons we have $\Sigma_{tot}^{</>} = \Sigma_L^{</>} + \Sigma_R^{</>}$, which vanish outside the band width the leads. On the other hand $\Delta^{</>}$ is only non-zero at energies corresponding to bound states, i.e. states lying outside the bands, and thus we conclude that the term (72) is always zero.

From Eqs. (69) and (70) it then follows that

$$\Delta I = \int \frac{\mathrm{d}\omega}{2\pi} \mathrm{Tr}\big[\Sigma^<(\omega)G_C^>(\omega) - \Sigma^>(\omega)G_C^<(\omega)\big]. \tag{73}$$

We notice that without any interactions particle conservation in the sense $\Delta I = 0$ is trivially fulfilled since $\Sigma = 0$. When interactions are present, particle conservation depends on the specific approximation used for the interaction self-energy, Σ.

4.4 Charge conservation from Φ-derivable self-energies

One expects that there should be a connection between the condition for particle conservation as expressed by $\Delta I = 0$ in Eq. (70), and the concept of a conserving approximation in the

Φ-derivable sense. Below we show that $\Delta I = 0$ is always obeyed when the self-energy is Φ-derivable.

We start by noting that Eq. (65) holds for *any* pair $G(1,2), \Sigma[G(1,2)]$ provided Σ is of the Φ-derivable form. In particular Eq. (65) does not assume that $G, \Sigma[G]$ fulfill a Dyson equation. Therefore, given any orthonormal, but not necessarily complete basis, $\{\phi_i\}$, and writing $G(1,2) = \sum_{ij} \phi_i(\mathbf{r}_1) G_{ij}(\tau_1, \tau_2) \phi^*(\mathbf{r}_2)$ we get from Eq. (65) after integrating over $\mathbf{r}_1$,

$$\sum_j \int_{\mathcal{C}} \mathrm{d}\tau' [\Sigma_{ij}(\tau, \tau') G_{ji}(\tau', \tau^+) - G_{ij}(\tau^-, \tau') \Sigma_{ji}(\tau', \tau)] = 0, \tag{74}$$

which in matrix notation takes the form

$$\int_{\mathcal{C}} \mathrm{d}\tau' \mathrm{Tr}[\Sigma(\tau, \tau') G(\tau', \tau^+) - G(\tau^-, \tau') \Sigma(\tau', \tau)] = 0. \tag{75}$$

Here Σ_{ij} is the self-energy matrix obtained when the diagrams are evaluated using G_{ij} and the $V_{ij,kl}$ from Eq. (3). The left hand side of Eq. (75), which is always zero for a Φ-derivable Σ, can be written as $\mathrm{Tr}[A^<(t,t)]$ when A is given by Eq. (92) with $B = \Sigma$ and $C = G$. It then follows from the general result (93) and the condition (73) that current conservation in the sense $I_L = -I_R$ is always obeyed when Σ is Φ-derivable.

The above derivation of Eq. (75) relied on *all* the Coulomb matrix elements, $V_{ij,kl}$, being included in the evaluation of Σ. Thus the proof does not carry through if a general truncation scheme for the interaction matrix is used. However, in the special case of a truncated interaction of the form (43), i.e. when the interaction is a two-point function, Eq. (75) remains valid. To show this, it is more appropriate to work entirely in the matrix representation and thus define $\Phi[G_{ij}(\tau, \tau')]$ as the sum of a set of skeleton diagrams evaluated directly in terms G_{ij} and $\tilde{V}_{ij}$. With the same argument as used in Eq. (64), it follows that Φ is invariant under the transformation

$$G_{ij}(\tau, \tau') \to e^{i\Lambda_i(\tau)} G_{ij}(\tau, \tau') e^{-i\Lambda_j(\tau')}, \tag{76}$$

where Λ is now a discrete vector. By adapting the arguments following Eq. (64) to the discrete case we arrive at Eq. (65) with the replacements $\mathbf{r}_1 \to i$ and $\mathbf{r}_2 \to j$ and with the integral replaced by a discrete sum over j. Summing also over i leads directly to Eq. (75) which is the desired result.

To summarize, we have shown that particle conservation in the sense $I_L = -I_R$, is obeyed whenever a Φ-derivable self-energy is used *and* either (i) all Coulomb matrix elements $V_{ij,kl}$ or (ii) the truncated two-point interaction of Eq. (43), are included in the calculation of Σ.

4.4.1 Example: Transport through a single level

As an illustrative example we consider transport through an Anderson impurity level connected to wideband leads, i.e. the retarded lead self-energies are taken to be frequency-independent equal to $i\Gamma$. The Hamiltonian of the central region reads

$$\hat{H}_C = \varepsilon_c c^\dagger c + U n_\uparrow n_\downarrow. \tag{77}$$

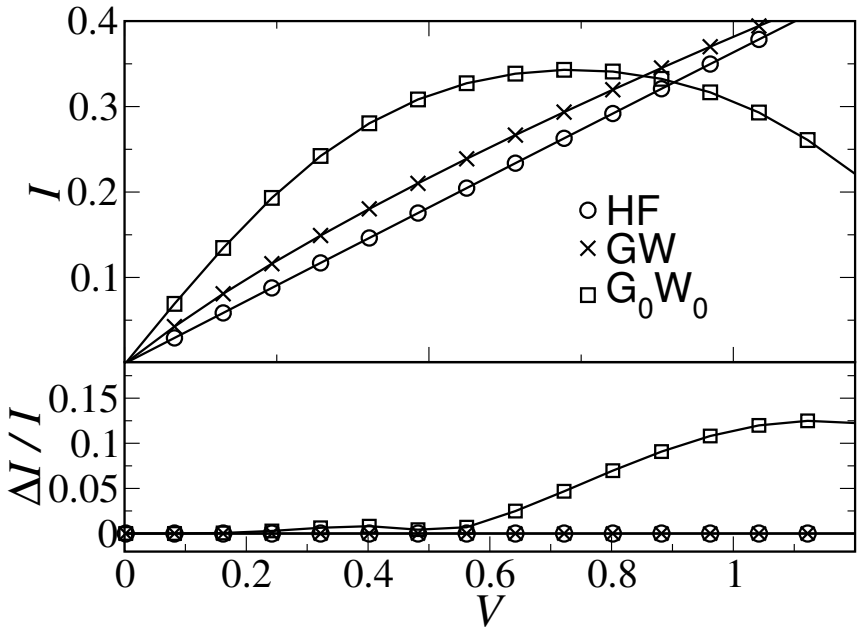

Figure 5: Current-voltage characteristic for an Anderson impurity level with $\Gamma = 0.65$, $\varepsilon_c = -4$, $U = 4$. At finite bias, the non-selfconsistent $G_0W_0[G_{\rm HF}]$ approximation yields different currents at the left and right interfaces ($\Delta I \neq 0$) which means that charge conservation is violated. Moreover, G_0W_0 predicts significant negative differential conductance for $V > 0.8$. In contrast, the Φ-derivable HF and GW self-energies both conserve charge.

where ε_c is the non-interacting energy and U is the correlation energy.

In Figure 5 we show the current-voltage curve calculated from Eq. (68) using the self-consistent HF, selfconsistent GW, and non-selfconsistent (NSC) GW approximations. The parameters used are given in the figure caption. In the NSC calculation (referred to as G_0W_0) we use the self-consistent Hartree-Fock GF to evaluate the GW self-energy. With this NSC self-energy we solve the Dyson's equation to obtain a NSC Green's function which is used to calculate the current. This "one-shot" approach is not conserving, and as a result the currents calculated in the left and right leads from Eq. (67) are not guaranteed to coincide. From the lower panel of figure 5 it can be seen that the G_0W_0 self-energy does indeed violate charge conservation, and moreover leads to unphysical negative differential conductance for $V > 0.8$. On the other hand the selfconsistent HF and GW approximations both conserve charge.

At this point we mention that the role of self-consistency in GW calculations has been much debated in the literature where it has been argued that G_0W_0, with G_0 being the DFT Green's function, produces better band structures and band gaps than self consistent GW. The present example clearly demonstrates that, regardless of the performance of GW for band structure calculations, self-consistency is fundamental in nonequilibrium situations.

5 TWO-LEVEL MODEL

In this section we apply the general formalism presented in the preceding sections to a generic two-level model of a molecular junction. In this model the molecule is represented by its highest occupied (HOMO) and lowest unoccupied (LUMO) orbitals and the leads are represented by one-dimensional tight-binding chains. With the aim of identifying universal trends we compare Hartree, Hartree-Fock, and GW calculations for the spectrum and IV characteristic. Not surprisingly the Hartree and HF results show large systematic differences due to the self-interaction errors in the Hartree potential. More interestingly, the dynamic correlations can have a large impact on both the spectrum and IV leading to significant deviations between the GW and HF results – in particular at finite bias.

In section 5.1 we introduce the two-level model. In section 5.2 we study how dynamic screening effects influence the equilibrium position of the HOMO and LUMO levels both in the case of weak and strong coupling between molecule and the leads. In section 5.3 we consider the nonequilibrium transport properties of the model and explain the features of the IV curves in terms of the variation of the HOMO and LUMO positions as a function of the bias voltage.

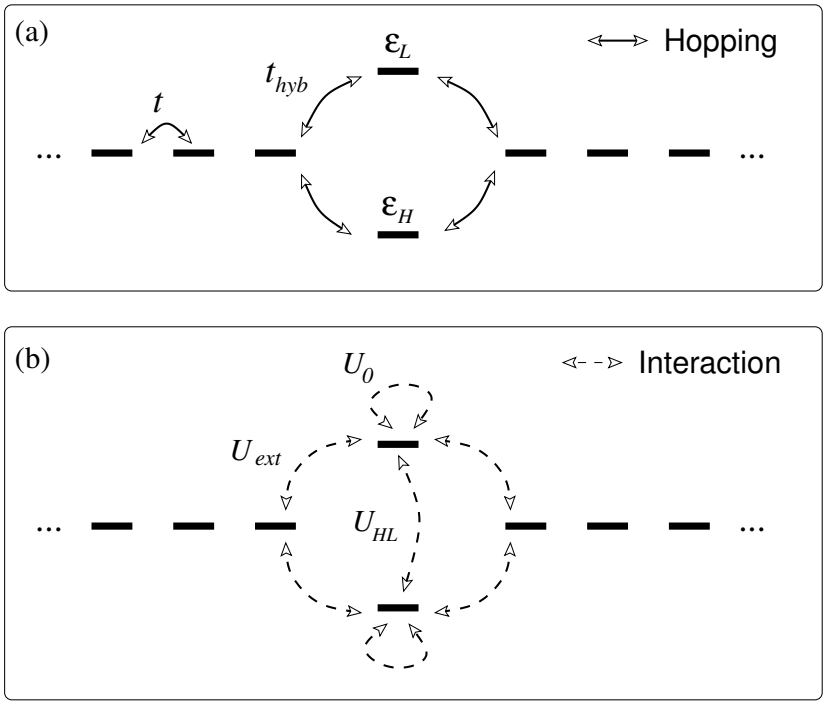

Figure 6: The two-level model used to describe the HOMO and LUMO levels of a molecule couped to metallic leads. (a) The one-particle hopping matrix elements. (b) The electron-electron interactions. The interactions can be divided into intra-molecule interactions (U_0 and U_{HL}) and metal-molecule interactions (U_{ext}).

5.1 Hamiltonian

The model consists of two electronic levels coupled to two semi-infinite 1D tight binding chains with nearest neighbor hopping, see Figure 6. The levels represent the HOMO and LUMO states of a molecule and the TB chains represent metallic leads. Electron-electron interactions on the molecule, and between the molecule and the first site of the chains are included. The Hamiltonian of the two-level model reads

$$\hat{H} = \hat{h}_l + \hat{h}_r + \hat{h}_{mol} + \hat{h}_{coup} + \hat{U}_{mol} + \hat{U}_{ext}. \tag{78}$$

Notice that we use a notation different from the canonical (L, C, R)-notation introduced in section 2. This is because of the requirement that all interactions must be contained in the central region. Due to the interactions between the molecule and first sites of the leads, this implies that the central region should at least comprise the molecule *and* the first two sites of the leads. We enumerate the sites of the TB leads from $-\infty$ to -1 (left lead), and from 1 to ∞ (right lead). Thus $\hat{h}_l$ reads

$$\hat{h}_l = \sum_{i=-\infty}^{-1} \sum_{\sigma=\uparrow,\downarrow} t(c^\dagger_{i\sigma} c_{i+1\sigma} + c^\dagger_{i+1\sigma} c_{i\sigma}) \tag{79}$$

with a similar expression for $\hat{h}_r$. The non-interacting part of the molecule's Hamiltonian reads

$$\hat{h}_{mol} = \sum_{\alpha=H,L} \sum_{\sigma=\uparrow,\downarrow} \xi_\alpha d^\dagger_{\alpha\sigma} d_{\alpha\sigma} \tag{80}$$

and the coupling is given by

$$\hat{h}_{coup} = \sum_{\alpha=H,L} \sum_{\sigma=\uparrow,\downarrow} t_{hyb}(c^\dagger_{1\sigma} d_{\alpha\sigma} + d^\dagger_{\alpha\sigma} c_{1\sigma} + c^\dagger_{-1\sigma} d_{\alpha\sigma} + d^\dagger_{\alpha\sigma} c_{-1\sigma}) \tag{81}$$

For clarity we use c-operators for the lead sites and d-operators for the HOMO/LUMO levels of the molecule. The interactions are given by

$$\hat{U}_{mol} = U_0(\hat{n}_{H\uparrow}\hat{n}_{H\downarrow} + \hat{n}_{L\uparrow}\hat{n}_{L\downarrow}) + U_{HL}\hat{n}_H\hat{n}_L \tag{82}$$

$$\hat{U}_{ext} = U_{ext}(\hat{n}_1\hat{n}_H + \hat{n}_1\hat{n}_L + \hat{n}_{-1}\hat{n}_H + \hat{n}_{-1}\hat{n}_L) \tag{83}$$

where e.g. $\hat{n}_H = d^\dagger_{H\uparrow} d_{H\uparrow} + d^\dagger_{H\downarrow} d_{H\downarrow}$ is the number operator of the HOMO level, and $\hat{n}_1$ is the number operator of the first site of the right lead. We set the Fermi level to zero corresponding to half-filled bands. In general, we write $\xi_L = \xi_H + \Delta_0$, i.e. we use the non-interacting energy gap as a free parameter. The occupation of the molecule can then be controlled by adjusting ξ_H.

5.2 Renormalization of molecular levels by dynamic screening

In the low-bias regime, the transport properties are to a large extent determined by the position of the HOMO and LUMO levels relative to the Fermi energy of the metal electrodes. For this reason we shall first consider how the HOMO and LUMO position are affected by the interactions in the zero bias limit. The material presented in this section is part of ongoing

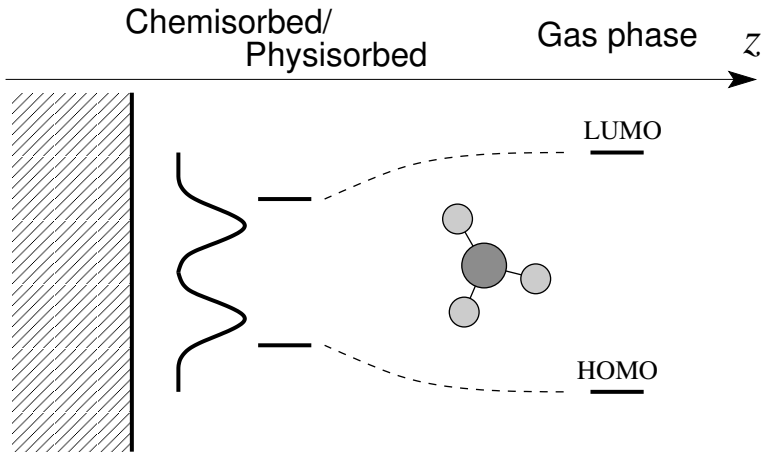

Figure 7: As a molecule approaches a metal surface its HOMO-LUMO gap is reduced by image-charge formation in the metal. If the molecule-metal bond is sufficiently strong (chemisorption) dynamic charge transfer between molecule and metal can give rise to additional reduction of the gap. These renormalization effects requires a dynamic, i.e. frequency dependent, self-energy and thus cannot be described within the single-particle picture.

work which will be published elsewhere.

When a molecule is brought into contact with a metal surface a number of different mechanisms will affect the position of the molecule's energy levels. First, the levels are shifted by the electrostatic potential outside the surface. Second, hybridization effects shift and broaden the levels into resonances with finite life-times. For our model, the resonance width due to coupling to the leads is $\Gamma \approx |t_{hyb}|^2/t$. Both the shift due to the surface potential and the hybridization are single-particle effects which can be described at a mean-field level such as Kohn-Sham (KS) or Hartree-Fock (HF) theory. On the other hand, correlation effects can renormalize the molecular spectrum in a way that cannot be described within a single-particle picture. Correlation effects are generally small for isolated molecules where HF usually yields good spectra, however, they can become significant when the molecule is in contact with a surface. An important example is the Kondo effect, where electronic interactions qualitatively changes the molecule's spectrum by introducing a narrow peak at the metal Fermi level (Goldhaber 1998 *et al.*, Costi *et al.* 1994, Thygesen and Rubio *et al.* 2008). In weakly correlated systems such as molecules with a closed shell structure adsorbed at a surface, the effect of electronic interactions is expected to be less dramatic. However, as we shall see below, dynamic screening at the molecule-metal interface can introduce significant reductions of the HOMO-LUMO gap, which in turn will influence the transport through the molecule. Such screening effects can be observed in photoemission- and electron tunneling spectroscopy (Johnson and Hulbert 1987, Kubatkin *et al.* 2003, Repp *et al.* 2005). Recently, first-principles *GW* calculations for benzene physisorbed on graphite showed a HOMO-LUMO gap reduction of more than 3 eV due to substrate polarization (Neaton *et al.* 2006). More empirical treatments of polarization/screening effects using a scissors operator on the DFT spectrum have recently been applied to transport in molecules (Quek *et. al* 2007 and Mowbray *et al.* 2008) and scanning tunneling microscopy simulations (Dubois *et al.* 2007). So far the theoretical studies have focused on weakly coupled (physisorbed) molecules where the gap

renormalization is induced by substrate polarization. This is the situation studied in section 5.2.2 below. In section 5.2.3 we consider the to the case of strongly coupled (chemisorbed) molecules.

5.2.1 The quasi-particle picture

In interacting many-electron systems the concept of a single-particle eigenenergy becomes meaningless. However, for weakly correlated systems the concept can still be maintained due to the long life-time of certain states of the form $c_m^\dagger|\Psi_0\rangle$ (for ϕ_m unoccupied) or $c_m|\Psi_0\rangle$ (for ϕ_m occupied). These quasiparticle (QP) states describes the many-body N-particle groundstate with and added electron (hole). The energy of the QP states relative to the groundstate energy, is given by the spectral function, $A_m(\varepsilon) = -\mathrm{Im}G^r_{mm}(\varepsilon)$, where G^r is the retarded Green's function. For weakly correlated systems $A_m(\varepsilon)$ will be peaked at the QP energy, ε_m, which is equivalent to saying that the QP has a long life-time. It is instructive to notice that the QP energies measures the cost of removing/adding an electron to the state $|\phi_m\rangle$ *in the presence* of interactions with the other electrons of the system.

For non-interacting electrons the peaks in the spectral function coincide with the eigenvalues of the single-particle Hamiltonian. Meanfield theories like KS or HF includes interactions at a static level, i.e. the single-particle eigenvalues correspond to the energy cost of adding/removing an electron when the state of all other electrons is kept fixed. This is the content of Koopman's theorem which states that (for ϕ_m occupied), $\varepsilon_m^{\mathrm{HF}} = E[\Phi_0^{\mathrm{HF}}] - E[c_m\Phi_0^{\mathrm{HF}}]$, i.e. the HF eigenvalues correspond to *unrelaxed* removal/addition energies. In general, the other electrons will respond to the added electron/hole and this will shift, or renormalize, the HF energies. The size of this effect is expected to qualitatively follow the linear response function, χ, which gives the change in the particle density when the system is subject to an external field,

$$\delta n(\mathbf{r};\omega) = \int \mathrm{d}\mathbf{r}\chi(\mathbf{r},\mathbf{r}';\omega)v_{\mathrm{ext}}(\mathbf{r}';\omega). \tag{84}$$

This suggests a direct relation between the impact of dynamic relaxations, or screening, on the QP spectrum, and the static response function $\chi(\omega = 0)$.

5.2.2 Weak molecule-lead coupling

We first consider the case of a weakly coupled, or physisorbed, molecule corresponding to small t_{hyb}. We use the following default parameter values: $t = 10$, $U_0 = 4$, $U_{HL} = 3$, $U_{ext} = 2$, $t_{hyb} = 0.3$, $\Delta_0 = 4$, which yield a resonance width of $\Gamma \approx 0.01$. In Fig. 8(left) we show the HOMO and LUMO positions as function of the interaction U_{ext} as calculated using the HF and GW approximations. As U_{ext} is increased corresponding to the molecule approaching the surface, the GW gap decreases while the HF gap remains unchanged. In the simplest picture the gap reduction is due to the interaction between the added/removed electron and its image charge in the metal. This effect is not present in the HF single-particle spectrum: According to Koopman's theorem the added/removed electron interacts with the HF groundstate of the neutral system which contains no image charge. For small t_{hyb} where the molecule's levels are well defined in energy and localized it is possible to include the response of the metal to the added/removed electron by performing HF total energy calculation with constrained

HOMO/LUMO occupation numbers. Denoting by Φ_0^n the minimizing Slater determinant with the constrain of n excess electrons on the molecule, we can define constrained HF energy levels as the total energy difference

$$\bar{\varepsilon}^{\rm HF}_{L/H} = \pm(E[\Phi_0^{\pm 1}] - E[\Phi_0^0]). \tag{85}$$

From the very good agreement between $\bar{\varepsilon}^{\rm HF}_n$ and ε^{GW}_n seen in Fig. 8b, we conclude that GW includes the effect of relaxation or screening in the metal at the HF level. The situation is sketched in Fig. 10a.

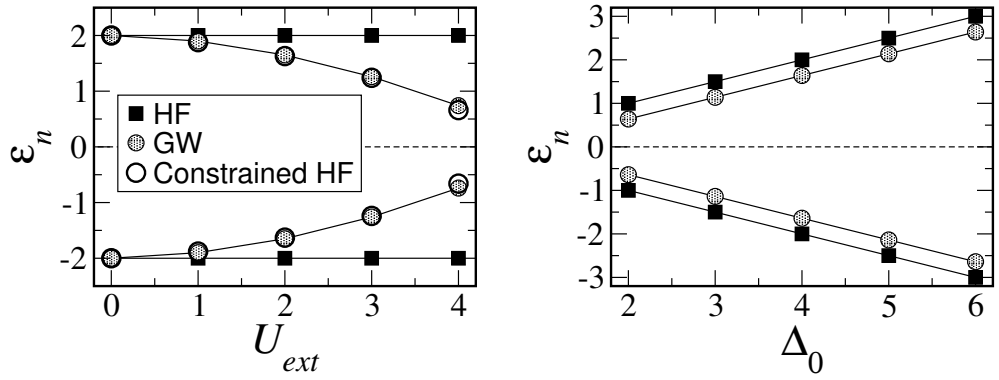

Figure 8: Position of the HOMO and LUMO levels as function of interaction strength U_{ext} (left) and non-interacting gap Δ_0 (right) for a weakly coupled molecule (small Γ). The GW HOMO (LUMO) correspond to the HF energy cost of removing (adding) an electron to the molecule when the Slater determinant of the metal is allowed to relax. The gap reduction from (unrelaxed) HF to GW is thus due to polarization of the metal. This gap reduction is independent of Δ_0.

Koopman's theorem allow us to write the difference between the HF single-particle levels and the result of constrained total energies, as (in case of the LUMO) $\varepsilon^{\rm HF}_L - \bar{\varepsilon}^{\rm HF}_L = E[\Phi_0^{+1}] - E[d_L^\dagger \Phi_0^0]$. This energy difference has two contributions: A positive one from the interaction between the added electron and the induced density in the metal, and a negative one being the cost of forming the induced density. The classical image charge approximation in contrast assumes perfect screening in the metal and zero energy cost of polarizing the metal.

From the right panel of Fig. 8 it can be seen that the renormalization of the gap is independent on the intrinsic gap of the molecule. This is expected since the image-charge and its interaction with the added electron/hole is independent on the HOMO-LUMO positions.

According to the above, the size of the gap reduction for fixed U_{ext} should depend on the polarizability of the metal. In Fig. 9(top) we show the dependence of the levels as function of t, i.e. the bandwidth of the metal. The effect is larger for small t corresponding to a narrow band. This is easily undestood by noting that narrow bands have larger DOS at ε_F which in turn implies a larger density response function. Indeed, the right panel of Fig. 9 shows the

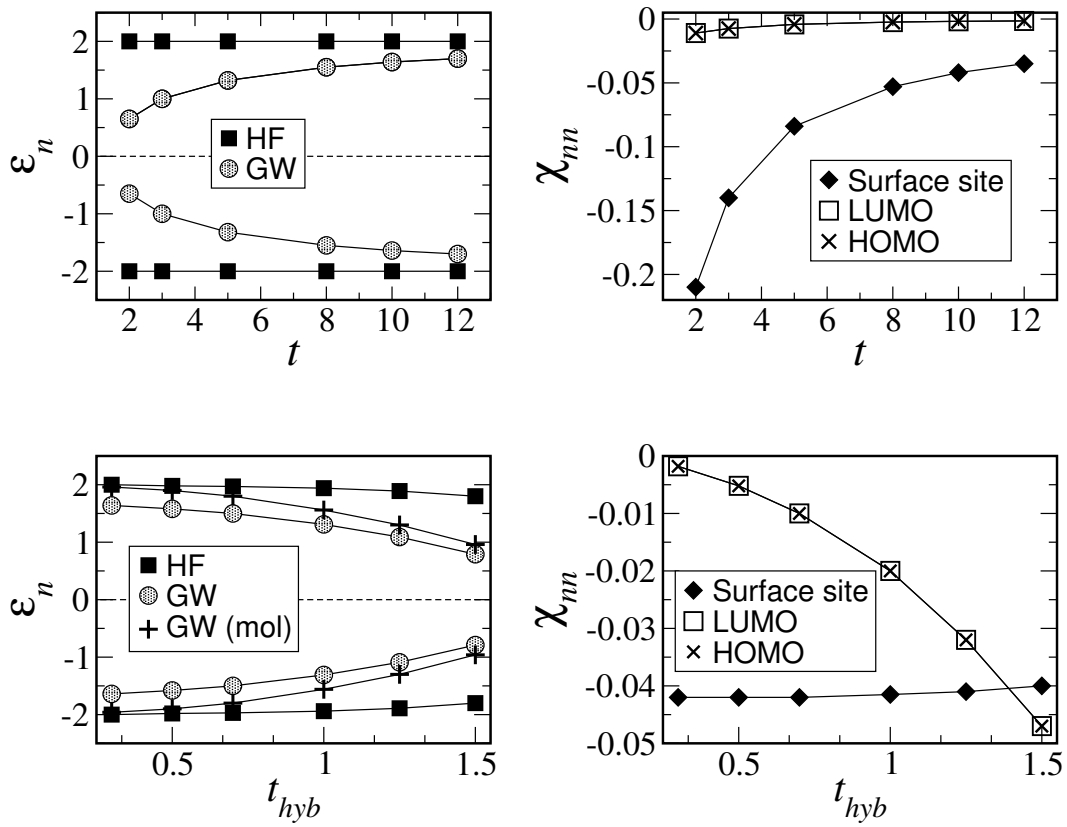

Figure 9: Left panels: Position of the molecule's HOMO and LUMO levels as a function of the metal bandwidth, t and the hybridization strength, t_{hyb}, respectively. GW(mol) refers to a calculation where only the interactions internally on the molecule have been treated within GW. Right panels: Static linear response functions (RPA) $\langle\phi_n|\chi(\omega=0)|\phi_n\rangle$ for the HOMO, LUMO and terminal site of the TB chain. The reduction of the correlated gap relative to HF is due to polarization of the metal and, for large t_{hyb}, of the molecule itself. Default parameter values are the same as in Fig.8

.

diagonal elements of the static (RPA) response function for the HOMO, LUMO and terminal site of the chain. The response function of the HOMO and LUMO is negligible for all values of t, while the response of the terminal site is significant and increases as t is reduced.

5.2.3 Strong molecule-lead coupling

We now turn to the case of a strongly coupled, or chemisorbed, molecule corresponding to non-negligible t_{hyb}. In the bottom panel of Fig. 9 we show the center of the molecular resonances as a function of t_{hyb}. In addition to the HF and GW values, we also show the result when only $\hat{U}_{mol}$ is treated at the GW level while $\hat{U}_{ext}$ is treated within HF. This allows us to isolate the correlation effects induced by the intra-molecular interactions from those of the metal-molecule interactions. Clearly, the correlated gap decrease relative to the HF gap as t_{hyb} is increased. It is also clear that the coupling-dependent part of the gap reduction comes from the interactions internally on the molecule, while the reduction due to $\hat{V}_{ext}$ is largely

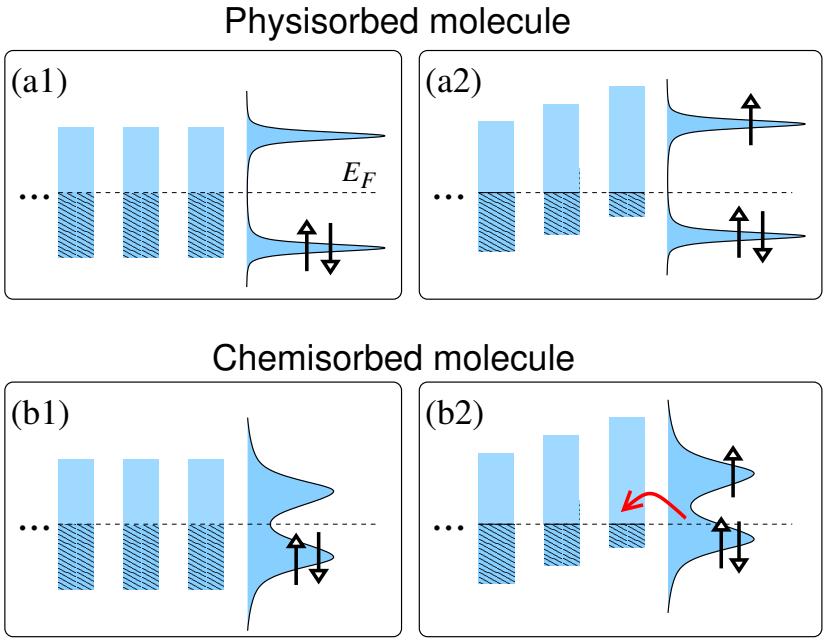

Figure 10: (a1) Groundstate of a physisorbed molecule at a metal surface. (a2) When an electron is added to the molecule, the metal is polarized. (b1) Groundstate of a chemisorbed molecule at a metal surface. (b2) When an electron is added to the LUMO the metal is polarized, and charge is transfered from the molecule to the metal. The screening effects stabilize the system with added/removed electron and this shift the occupied (unoccupied) quasi-particle levels up (down).

independent of t_{hyb}. Since $\hat{V}_{mol}$ does not produce any renormalization of the levels of the free molecule (see the $t_{hyb} \to 0$ limit), the mechanism responsible for the gap reduction must involve the metal. From the lower right panel of Fig. 9, we see that the response functions of the HOMO and LUMO states increases with t_{hyb} indicating the gap reduction due to $\hat{V}_{mol}$ is of a similar nature as the image charge effect, but with the molecule itself being polarized. The effect increases with t_{hyb} because charge transfer between the molecule and the metal due to the external field from the added/removed electron, is larger when resonances are broad and have larger overlap with the metal Fermi level. The situation is sketched in Fig. 10b.

5.3 Nonequilibrium transport

The analysis of the previous sections show that dynamic screening effects can have a large effect on the spectrum of the molecule in contact with leads. In this section we shall see that the application of a bias voltage leads to additional renormalization of the spectrum. For simplicity we limit the model to include intra-molecule interactions, i.e. we set U_{ext} to zero. This means that reduction of the HOMO-LUMO gap due to image charge formation in the leads is not included. Whereas the presence of intra-molecule interactions did not have a large influence on the equilibrium positions of the HOMO and LUMO levels for small values of Γ (see the GW(mol) result in Fig. 9), we will see that this is no longer true under finite bias conditions, where intra-molecular screening is strongly enhanced and the life-times of the HOMO and LUMO levels can be significantly reduced due to QP scattering. Both effects lead

to a reduction of the HOMO-LUMO gap as function of the bias voltage with a large impact in the calculated IV curve.

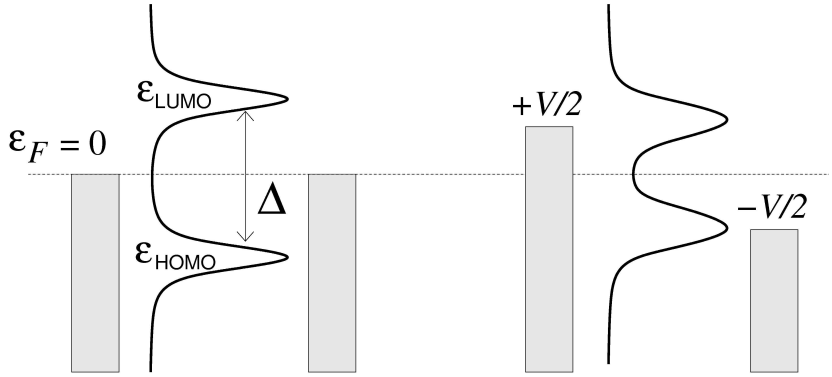

Figure 11: The HOMO and LUMO resonances of the two-level model under zero and non-zero bias voltage. As indicated the bias affects both the position and width of the resonances and this will in turn affect the dI/dV curve. Reprinted with permission from Thygesen, Phys. Rev. Lett. **100**, 166804 (2008). Copyright 2008 by the American Physical Society.

Throughout this section we use following parameters: $\Delta_0 = 2$, $U_0 = 2$, $U_{HL} = 1.5$, $t = 10$. By varying the one-particle energy ξ_0, we can control the equilibrium occupation of the molecule, $N_{\rm el}$. We consider the case of weak charge transfer to the molecule, i.e. $N_{\rm el}$ ranges from 2.0 to 2.1, corresponding to ε_F lying in the middle of the gap and slightly below the LUMO, respectively. The Fermi level is set to zero, and the bias is applied symmetrically, i.e. $\mu_L = V/2$ and $\mu_R = -V/2$. The situation is illustrated in figure 11.

In Fig. 12 we show the calculated dI/dV curves (obtained by numerical differentiation of $I(V)$) for different values of Γ and $N_{\rm el}$. We first notice that the $2B$ and GW approximations yield similar results in all the cases indicating that the higher order terms in the GW self-energy are fairly small. For $\Gamma = 1.0$, all methods yield qualitatively the same result. For even larger values of Γ (not shown), and independently of $N_{\rm el}$, the results become even more similar. In this strong coupling limit, single-particle hybridization effects will dominate over the interactions and xc-effects are small.

Focusing on the $\Gamma = 0.25$ case we see that the Hartree approximation severely overestimates the low-bias conductance. This is a consequence of the self-interactions (SI) contained in the Hartree potential which leads to an underestimation of the (equilibrium) HOMO-LUMO gap, see figure 13 for $V = 0$. On the other hand the HF, 2B, and GW methods lead to very similar conductances in the low-bias regime. This is consistent with the results of the previous section which showed that intra-molecular correlations do not renormalize the equilibrium HF gap much for small Γ. For $\Gamma = 1.0$ the slightly larger conductance in GW and 2B is due to the slight reduction of the equilibrium gap.

We notice that the lower left graph ($\Gamma = 0.25$, $N_{\rm el} = 2.0$) shows an interesting feature.

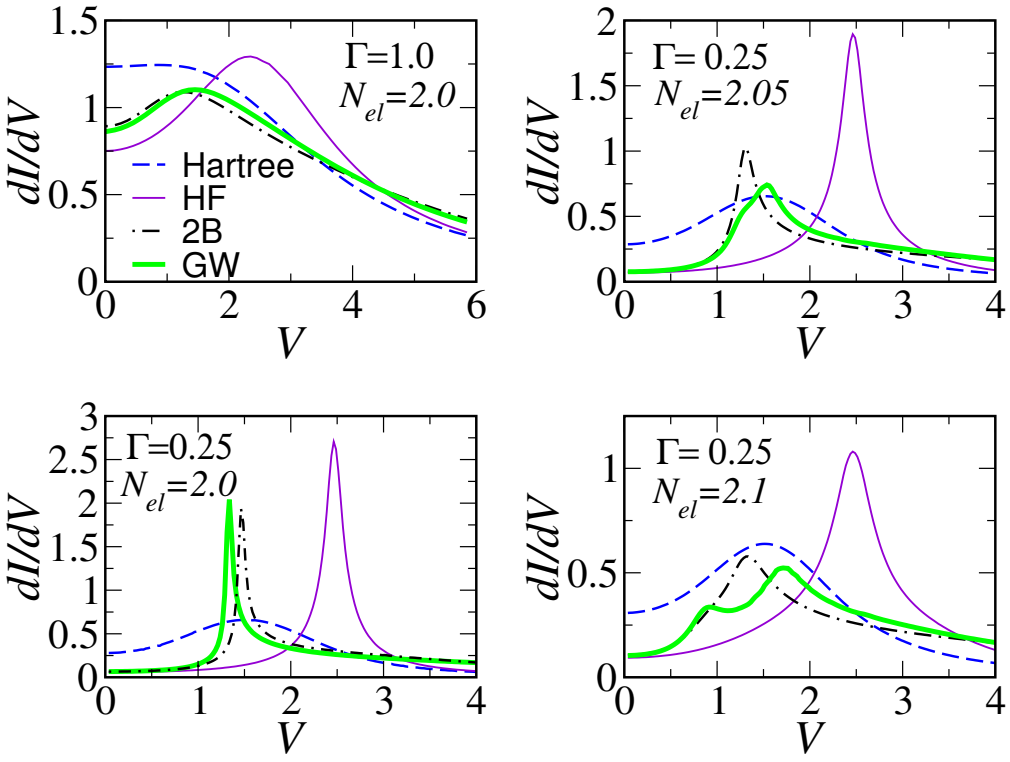

Figure 12: dI/dV curves for different values of the tunneling strength Γ and occupation of the molecule, $N_{\rm el}$. The curves are calculated using different approximations for the xc self-energy. Reprinted with permission from Thygesen, Phys. Rev. Lett. **100**, 166804 (2008). Copyright 2008 by the American Physical Society.

Namely, the HF, 2B, and GW curves all contain an anomalously strong conductance peak. Interestingly, the peak height is significantly larger than 1 which is the maximum conductance for a single level (the Anderson impurity model). Moreover, the full width at half maximum (FWHM) of the peak is only $\sigma_{\rm HF} = 0.27$ and $\sigma_{\rm 2B/GW} = 0.12$, respectively, which is much smaller than the tunneling broadening of $2\Gamma = 0.5$. We note in passing that the peak looses intensity as $N_{\rm el}$ is increased, and that the Hartree approximation does not reproduce the narrow peak.

5.3.1 Influence of bias on the HOMO and LUMO positions

To understand the origin of the anomalous conductance peaks, we consider the evolution of the HOMO and LUMO positions as a function of the bias voltage, see Fig. 13 (the 2B result is left out as it is similar to GW). Focusing on the upper panel of the figure (corresponding to $N_{\rm el} = 2.0$), we notice a qualitative difference between the Hartree and the SI-free approximations: While the Hartree gap expands as the levels move into the bias window, the HF and GW gaps shrink leading to a dramatic increase in current around $V = 2.5$ and $V = 1.3$, respectively. This is clearly the origin of the anomalous dI/dV peaks. But why do the SI-free gaps shrink as the bias is raised?

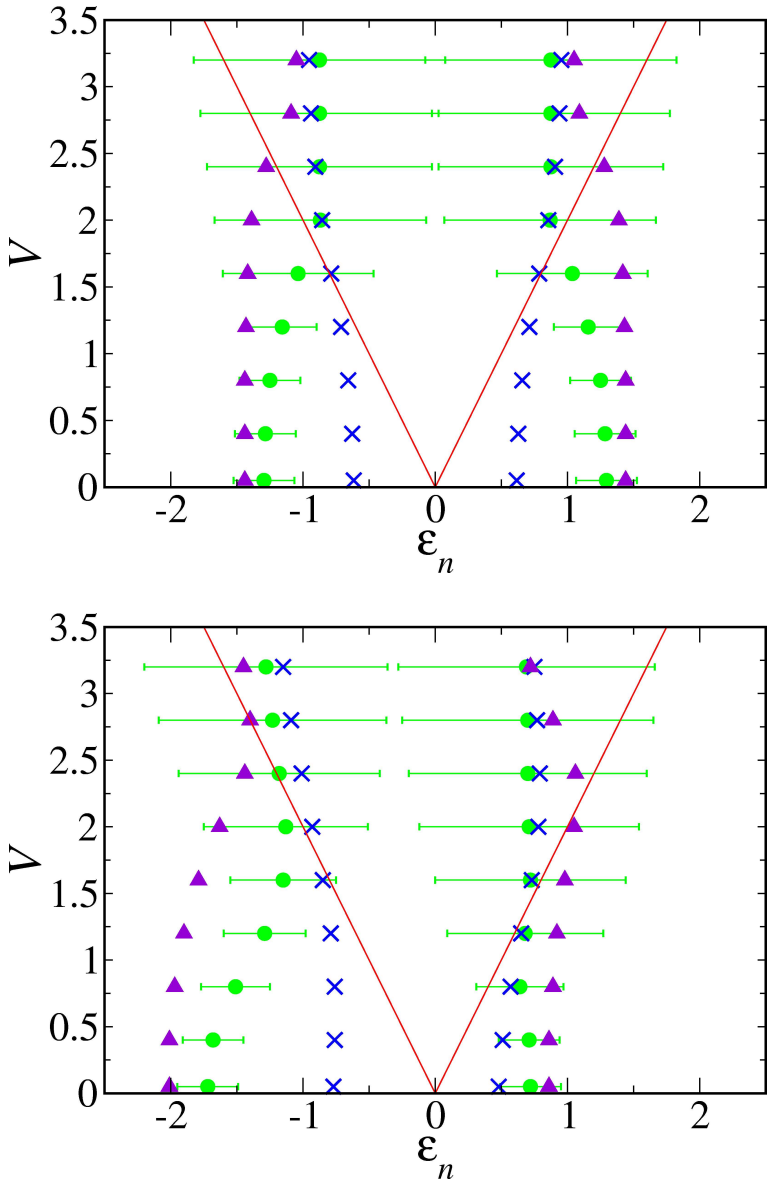

Figure 13: Position of the HOMO and LUMO levels as a function of the bias voltage for the Hartree (crosses), HF (triangles), and GW (circles) approximations. The horizontal lines show the FWHM of the GW resonances. The FWHM of the Hartree and HF resonances is 2Γ independently of V. Notice the differences in the way the levels enter the bias window: The Hartree gap opens while the HF and GW gaps close. In the upper graph $\Gamma = 0.25$, $N_{\rm el} = 2.0$ (symmetric case). In the lower graph $\Gamma = 0.25$, $N_{\rm el} = 2.1$. Reprinted with permission from Thygesen, Phys. Rev. Lett. **100**, 166804 (2008). Copyright 2008 by the American Physical Society.

Let us consider the change in the HOMO and LUMO positions when the bias V is increased by $2\delta V$. In general this change must be determined self-consistently, however, a "first iteration" estimate yields a change in the HOMO and LUMO occupations of $\delta n_H \approx -A_H(-V/2)\delta V$ and $\delta n_L \approx A_L(V/2)\delta V$, respectively. Here $A_{H/L}$ is the spectral function, or

equivalently the DOS, of the HOMO/LUMO levels. At the HF level this leads to

$$\delta\varepsilon_H \approx [-U_0 A(-V/2) + 2U_{HL} A(V/2)]\delta V \quad (86)$$
$$\delta\varepsilon_L \approx [U_0 A(V/2) - 2U_{HL} A(-V/2)]\delta V \quad (87)$$

where $A = H_H + A_L$ is the total DOS on the molecule and we have used that $A_H(-V/2) \approx A(-V/2)$ and $A(V/2) \approx A(V/2)$. The factor 2 in front of U_{HL} accounts for interactions with both spin channels. In the symmetric case ($N_{\rm el} = 2.0$) we have $A(-V/2) = A(V/2)$. Since $U_0 < 2U_{HL}$ this means that $\delta\varepsilon_H > 0$ and $\delta\varepsilon_L < 0$, i.e. the gap is reduced as V is raised. Moreover it follows that the gap reduction is largest when $A(\pm V/2)$ is largest, that is, just when the levels cross the bias window. In the general case ($N_{\rm el} \neq 2.0$) the direction of the shift depends on the relative magnitude of the DOS at the two bias window edges: a level will follow the edge of the bias window if the other level does not intersect the bias edge. It will move opposite to the bias, i.e. into the bias window, if the other level is close to the bias window edge. This is effect clearly seen in the lower graph of Fig. 13 (triangles). Thus the gap closing mechanism has the largest impact on the dI/dV curve when the HOMO and LUMO levels hit the bias window simultaneously. Moreover, the effect is stronger the larger U_{HL}/U_0, and the smaller Γ (the maximum in the DOS is $\sim 1/\Gamma$). At the Hartree level, Eqs. (86) and (87) are modified by replacing U_0 by $2U_0$ due to self-interaction. This leads to an effective pinning of the levels to the bias window which tends to open the gap as V is increased, see Fig. 13 (crosses).

The above analysis shows why the HF gap is reduced as the levels hit the bias window. Interestingly, the bias-driven gap reduction is even stronger in GW and as a consequence the GW conductance peak occurs at much lower bias ($V = 1.5$) than the HF peak ($V = 2.5$). Part of the downshift of the GW conductance peak can be explained from the smaller GW equilibrium gap. Indeed, for $V = 0$ the HF gap is ~ 0.3 larger than the GW gap. However, this effect alone cannot account for the large down-shift.

The reason for the bias induced reduction of the GW gap is two-fold: First, intra-molecular screening effects are enhanced as the chemical potentials move closer to the molecular levels and increase the susceptibility of the levels. This is analogue to the (equilibrium) situation of increasing Γ shown in lower panels of figure 9. The susceptibility of a molecular level is roughly given by the magnitude of the level's DOS at E_F (or chemical potentials). In the latter case this is achieved by broadening the resonances; in the former case by bringing the chemical potential(s) closer to the levels. Secondly, the rate of QP scattering, i.e. the rate at which the initial state $c_i^\dagger|\Psi_0\rangle$ is destroyed due to electron-electron interactions, increases with the bias. This follows from Fermi's Golden rule by realizing that the number of available final states of the form $c_f^\dagger|\Psi_0\rangle$ having the same energy as the initial state, increases with bias. The enhanced QP scattering reduces the life-time of the HOMO and LUMO QPs, which is equivalent to a broadening of the molecular resonances.

The full width at half maximum (FWHM) of the GW resonances is indicated by horizontal lines in Fig. 13. For low bias, the width of the GW resonances is the same as the width of the Hartree and HF resonances. The latter is determined by the coupling to leads and equals $2\Gamma = 0.5$ independently of the bias. According to Fermi-liquid theory, QP scattering at the Fermi level is strongly suppressed in the ground state, i.e. $\mathrm{Im}\Sigma_{ii}(\varepsilon_F) = 0$ for $V = 0$ (recall

that ImΣ is inversely proportinal to the life time). However, as the bias is raised the phase space available for QP scattering is enlarged and ImΣ increases accordingly. As a result of the additional level broadening, $A(\pm V/2)$ increases more rapidly as a function of V. According to Eqs.(86,87), this will accelerate the gap closing reduction already at the HF level. Finally, we notice that the long, flat tails seen in the dI/dV of the GW/2B calculations are also a result of the spectral broadening due to QP scattering.

6 PROTOTYPE MOLECULAR JUNCTIONS: C_6H_6 and H_2

In this section we combine the GW scheme with a Wannier function (WF) basis set to study electron transport through two prototypical junctions, namely a benzene molecule coupled to featureless leads and a hydrogen molecule between two semi-infinite Pt chains. In section 6.1 we briefly present the computational scheme. In the following two sections we analyze the energy spectrum and transport properties of the benzene junction. Finally in section 6.4 we present results for the IV curve of the Pt-H_2-Pt junction.

6.1 Computational details

Below we review our computational scheme for GW transport calculations in a WF basis discussed in detail in Thygesen and Rubio 2008. In a first step, periodic supercell DFT calculations are performed for the leads as well as the central region containing the molecule plus part of the leads. We use the Dacapo code (Bahn and Jacobsen 2002) which applies ultrasoft pseudopotentials (Vanderbilt 1990) for the ion cores. The KS eigenstates are expanded in plane waves with a cut off energy of 340 Ry and the PBE xc-functional (Perdew *et al.* 1996) is used. In the second step, the KS eigenstates are transformed into maximally localized, partially occupied WFs, $\{\phi_n(\mathbf{r})\}$, and the KS Hamiltonians of the central region and the leads are subsequently evaluated in terms of the WF basis. The eighteen maximally localized WFs obtained for the benzene molecule are shown in Fig. 14. The xc-potential is excluded from the Hamiltonian of the central region in order to avoid double counting when the GW self-energy is added. The central region Hamiltonian reads

$$[h_C]_{ij} = \langle \phi_i | -\frac{1}{2}\nabla^2 + v_{ps} + v_h | \phi_j \rangle, \tag{88}$$

where v_{ps} is the pseudopotential and v_h is the Hartree potential. Notice that v_{ps} and v_h contain contributions from the ion cores and electron density of the leads as they are obtained from a supercell calculation with part of the leads included.

The Coulomb integrals are evaluated for the WFs of the central region,

$$V_{ij,kl} = \int\int \mathrm{d}\mathbf{r}\mathrm{d}\mathbf{r}' \frac{\phi_i(\mathbf{r})^*\phi_j(\mathbf{r}')^*\phi_k(\mathbf{r})\phi_l(\mathbf{r}')}{|\mathbf{r}-\mathbf{r}'|}. \tag{89}$$

For the correlation part of the GW self-energy, $\Sigma_{\mathrm{corr}} = \Sigma_{GW} - \Sigma_x$, we use the effective interaction introduced in section 3.1, i.e. only Coulomb integrals of the form $V_{ij,ij}$ and $V_{ij,ji}$ are included. For the Hartree and exchange self-energies, Σ_h and Σ_x, which are easily evaluated from Eqs. (58,59), we use all the Coulomb matrix elements. Notice, that we need Σ_h even though the Hartree potential from electrons in C is already contained in v_h. The reason is

that the latter is the equilibrium Hartree potential of the DFT calculation, which might well differ from the Hartree potential of a nonequilibrium GW calculation.

The retarded Green's function is evaluated from

$$G^r = [\omega - h_C - \Sigma_L - \Sigma_R - (\Sigma_h^r[G] - \Sigma_h^r[g_s^{(\mathrm{eq})}]) - \Sigma_{xc}^r[G]]^{-1}, \tag{90}$$

where the frequency dependence has been omitted for notational simplicity. Several comments are in order. First, Σ_L and Σ_R are the lead self-energies of Eq. (41) (in the wide-band approximation Σ_L and Σ_R are diagonal and frequency independent). The term $\Delta v_h \equiv \Sigma_h^r[G] - \Sigma_h^r[g_s^{(\mathrm{eq})}]$ is the change in Hartree potential relative to the equilibrium DFT value. This change is due to the applied bias and the replacement of v_{xc} by Σ_{xc}. In this work Σ_{xc} can be either the exchange or the GW self-energy. Finally we notice that the bias dependence of the various quantities entering Eq. (90) has been suppressed for notational simplicity.

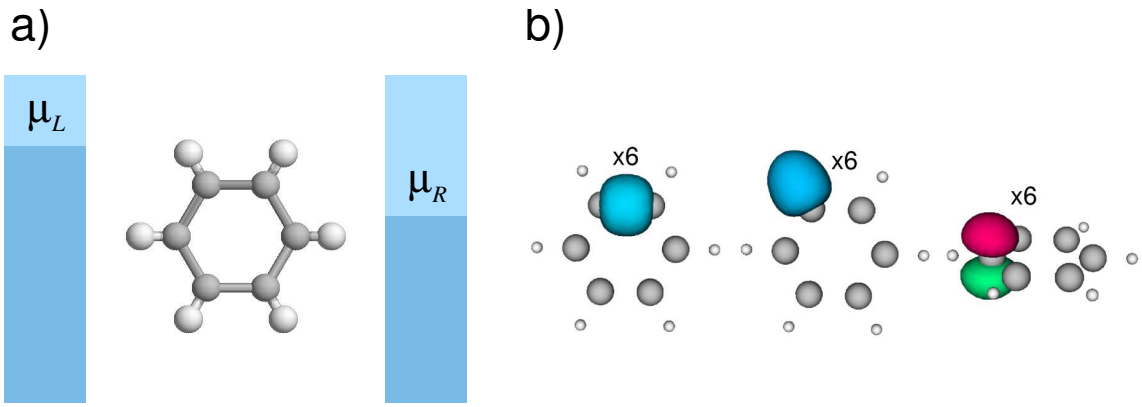

Figure 14: (a) Illustration of a benzene molecule coupled to featureless electrodes with different chemical potentials. (b) Iso-surfaces for the 18 partially occupied Wannier functions used as basis functions in the calculations. The WFs are linear combinations of Kohn-Sham eigenstates obtained from a DFT-PBE plane-wave calculation.

6.2 Equilibrium spectrum of benzene

In Fig. 15 we show the total density of states (DOS) of the isolated benzene molecule calculated using three different approximations: (i) DFT-PBE (ii) Hartree-Fock (iii) fully self-consistent GW. The DOS is given by

$$D(\varepsilon) = -\frac{1}{\pi}\sum_{n=1}^{N_w} \mathrm{Im} G_{nn}^r(\varepsilon), \tag{91}$$

where the sum runs over all WFs on the molecule, and the GF is obtained from Eq. (90) using a wide-band lead self-energy of $\Gamma = 0.05$. We stress that our calculations include the full dynamic dependence of the GW self-energy as well as all off-diagonal elements. Thus no analytical extension is performed, and we do not linearize the self-energy around the DFT eigenvalues to obtain an approximate quasi-particle equation as is done in standard GW calculations.

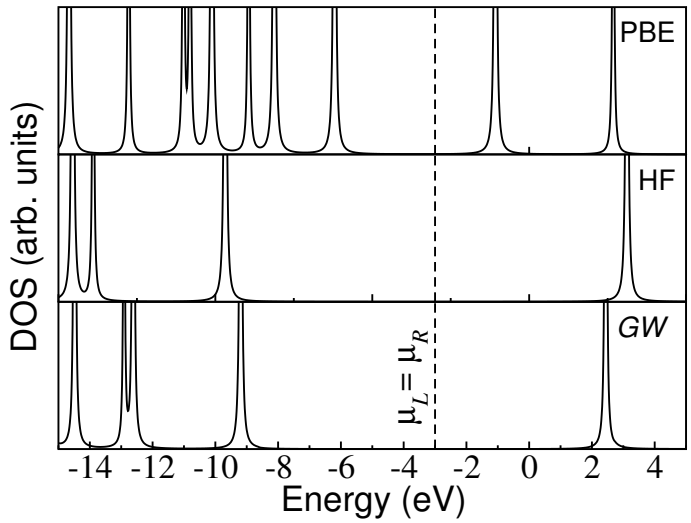

Figure 15: Density of states for a benzene molecule weakly coupled to featureless leads ($\Gamma = 0.05$). The common Fermi levels of the leads is indicated. Notice the characteristic opening of the band gap when going from DFT-PBE to HF, and the subsequent (slight) reduction when correlations are included at the *GW* level. Reprinted with permission from Thygesen and Rubio, Phys. Rev. B **77**, 115333 (2008). Copyright 2008 by the American Physical Society.

The spectral peaks seen in Fig. 15 occurring above (below) the Fermi level correspond to electron addition (removal) energies. In particular, the HOMO level should coincide with the ionization potential of the isolated molecule, which in the case of benzene is $I_{\rm exp} = -9.2$ eV (NIST Chemistry WebBook). The PBE functional overestimates this value by 3 eV, giving $I_{\rm PBE} = -6.2$ eV in good agreement with previous calculations (Niehaus *et al.* 2005). The HF and *GW* calculation yields $I_{\rm HF} = -9.7$ eV and $I_{GW} = -9.3$ eV, respectively. Given the limited size of the Wannier basis, the precise values should not be taken too strict. However, the results demonstrate the general trend: KS theory with a local xc-functional underestimates the HOMO-LUMO gap significantly due to SI errors; HF overestimates the gap slightly; *GW* reduces the HF gap slightly through the inclusion of dynamic screening.

In Fig. 16 we plot the size of the HOMO-LUMO gap as a function of the coupling strength Γ. The position of the levels has been defined as the first maximum in the DOS to the left and right of the Fermi level. Both the HF and *GW* gaps decrease as Γ is increased. This observation is consistent with the model calculations of section 5.2.3 where it was found that the gap reduction due to the correlation part of the *GW* self-energy, $\Delta_{\rm corr}$, can be understood as a virtual charge transfer between molecule and leads. The reduction of the HF gap as function of Γ is a consequence of the redistribution of charge from the HOMO to the LUMO when the resonances broaden and their tails start to cross the Fermi level. This is completely analogue to the bias induced gap reduction discussed in section 5.3. These results for benzene show that the conclusions obtained from the two-level model apply to more realistic systems.

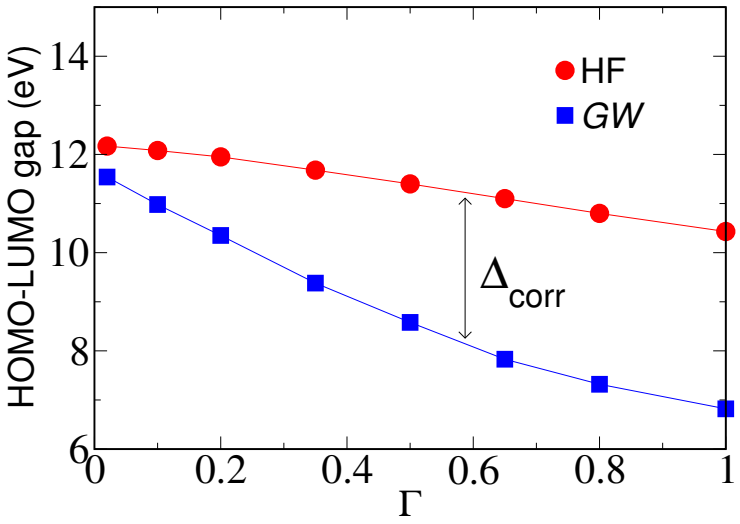

Figure 16: The HF and GW HOMO-LUMO gap of the benzene molecule as a function of the coupling strength Γ. The difference between the curves represents the reduction in the gap due to the correlation part of the GW self-energy. This value increases with the coupling strength, as polarization of the molecule via dynamic charge transfer to the metal becomes possible (see section 5.2.3). Reprinted with permission from Thygesen and Rubio, Phys. Rev. B **77**, 115333 (2008). Copyright 2008 by the American Physical Society.

6.3 Conductance of benzene

We consider electron transport through the benzene junction under a symmetric bias, $\mu_{L/R} = \pm V/2$, and a wide-band coupling strength of $\Gamma_L = \Gamma_R = 0.25$ eV. In Fig. 17 we compare the differential conductance, $\mathrm{d}I/\mathrm{d}V$, calculated from self-consistent DFT-PBE, HF, and GW, as well as non self-consistent G_0W_0 using either the DFT-PBE or HF Green's function as G_0. The $\mathrm{d}I/\mathrm{d}V$ has been obtained by numerical differentiation of the $I(V)$ curves calculated from Eq. (68). For the DFT calculation the finite-bias effects have been included at the Hartree level, i.e. changes in the xc-potential have been neglected. We notice that the HF and $G_0W_0[G_{\mathrm{HF}}]$ results are close to the self-consistent GW result. These approximations all yield a nearly linear IV with a conductance of $\sim 0.05G_0$. In contrast the DFT and $G_0W_0[G_{\mathrm{DFT}}]$ yield significantly larger conductances which increase with the bias voltage. We note that the violation of charge conservation in the G_0W_0 calculations is not too large in the present case ($\Delta I/I < 5\%$). This is in line with our general observation, e.g. from the Anderson model, that $\Delta I/I$ increases with I.

The trends in conductance can be understood by considering the (equilibrium) DOS of the junction shown in Fig. 18. As for the weakly-coupled (free) benzene molecule whose spectrum is shown in Fig. 15, the DFT HOMO-LUMO gap is much smaller than the HF gap, and this explains the larger DFT conductance. The GW gap falls in between the DFT and HF gaps, however, the magnitude of the DOS at E_F is very similar in GW and HF which is the reason

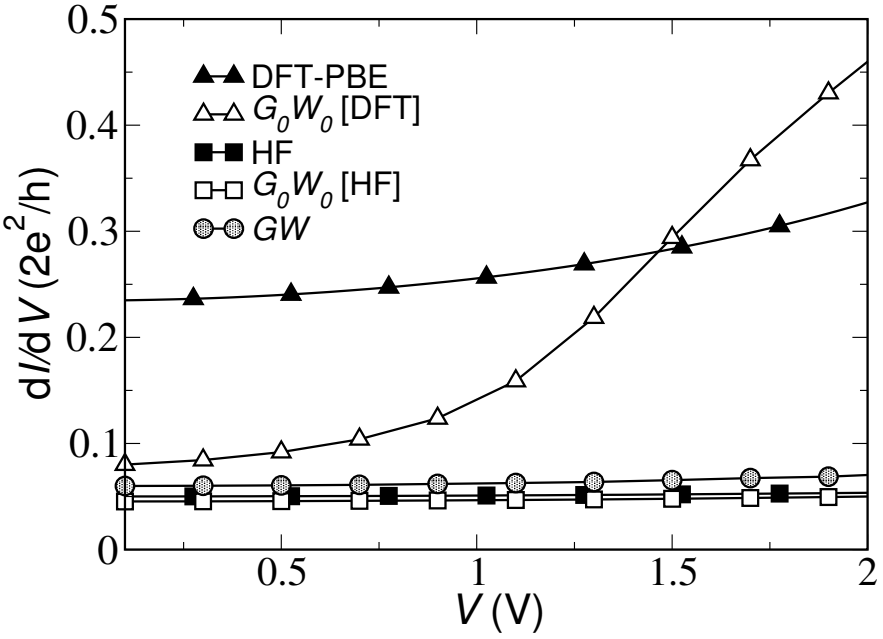

Figure 17: Differential conductance of the benzene junction for $\Gamma_L = \Gamma_R = 0.25$ eV. Notice the strong G_0 dependence of the G_0W_0 result. Reprinted with permission from Thygesen and Rubio, Phys. Rev. B **77**, 115333 (2008). Copyright 2008 by the American Physical Society.

for the similar conductances. It is interesting to notice that the HOMO-LUMO gap obtained in the G_0W_0 calculations resemble the gap obtained from G_0, and that the self-consistent GW gap lies in between the $G_0W_0[G_{\rm DFT}]$ and $G_0W_0[G_{\rm HF}]$ gaps.

The increase in the $G_0W_0[G_{\rm DFT}]$ conductance as a function of bias occurs because the LUMO of the $G_0W_0[G_{\rm DFT}]$ calculation moves downwards into the bias window and becomes partly filled as the voltage is raised. In a self-consistent calculation this would lead to an increase in Hartree potential which would in turn raise the energy of the level. The latter effect is missing in the perturbative G_0W_0 approach and this can lead to uncontrolled changes in the occupations as the present example shows.

Finally, we notice that the $G_0W_0[G_{\rm DFT}]$ DOS is significantly more broadened than both the $G_0W_0[G_{\rm HF}]$ and GW DOS. The reason for this is that, as a direct consequence of the small HOMO-LUMO gap, DFT yields a the larger DOS close to E_F. The larger DOS in turn enhances the QP scattering and leads to shorter life-times of the QP in the $G_0W_0[G_{\rm DFT}]$ calculation. Since the QP life-time is inversely proportional to $\mathrm{Im}\Sigma_{GW}$ this explains the broadening of the spectrum.

6.4 Pt-H_2-Pt junction

We consider a molecular hydrogen bridge between infinite atomic Pt chains as shown in the inset of Fig. 19. Experimentally, the conductance of the hydrogen junction is found to be

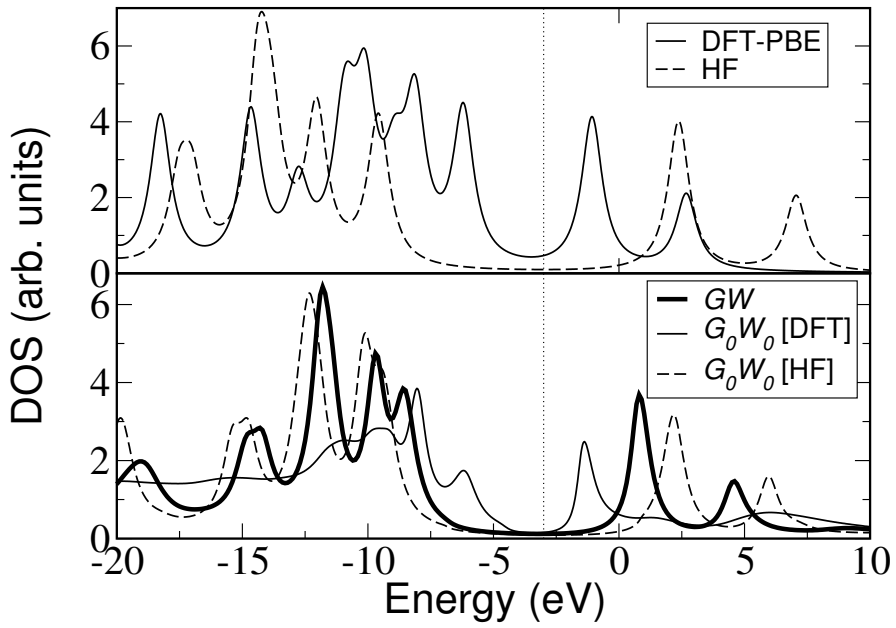

Figure 18: Equilibrium DOS for the benzene molecule coupled to wide-band leads with a coupling strength of $\Gamma_L = \Gamma_R = 0.25$ eV. Upper panel shows DFT-PBE and HF single-particle approximations while the lower panel shows the self-consistent GW result as well as one-shot G_0W_0 results based on the DFT and HF Green's functions, respectively. Reprinted with permission from Thygesen and Rubio, Phys. Rev. B **77**, 115333 (2008). Copyright 2008 by the American Physical Society.

close to the conductance quantum, $G_0 = 2e^2/h$ (Smit *et al.* 2002), and this value has been reproduced by DFT calculations (Thygesen and Jacobsen 2005). Below we present GW-transport results for a simplified model of this system (using infinite Pt chains as leads), and refer to Thygesen and Rubio 2007 for further details on the calculations.

In the upper panel of Fig. 19 we show the local density of states (LDOS) at one of the two H orbitals as calculated within DFT using the PBE xc-functional, as well as self-consistent HF (in the central region). In DFT the H_2 bonding state is a bound state at -7.0 eV relative to E_F, while the anti-bonding state lies at 0.4 eV and is strongly broadened by coupling to the Pt. Moving from DFT to HF the bonding state is shifted down by ~ 8 eV because for occupied states the exchange potential is more negative than the DFT xc-potential. The same effect tends to drive the half-filled anti-bonding state down but in this case the resulting increase in the Hartree potential (about 4 eV) stops it just below E_F.

In the lower panel of Fig. 19 we show the LDOS calculated in GW as well as G_0W_0 starting from either DFT or HF, i.e. G_0 is either $G_{\rm DFT}$ or $G_{\rm HF}$. The large deviation between the two G_0W_0 results is not surprising given the large difference between $G_{\rm DFT}$ and $G_{\rm HF}$. A closer analysis of the origin of this deviation can be found elsewhere (Thygesen and Rubio 2007).

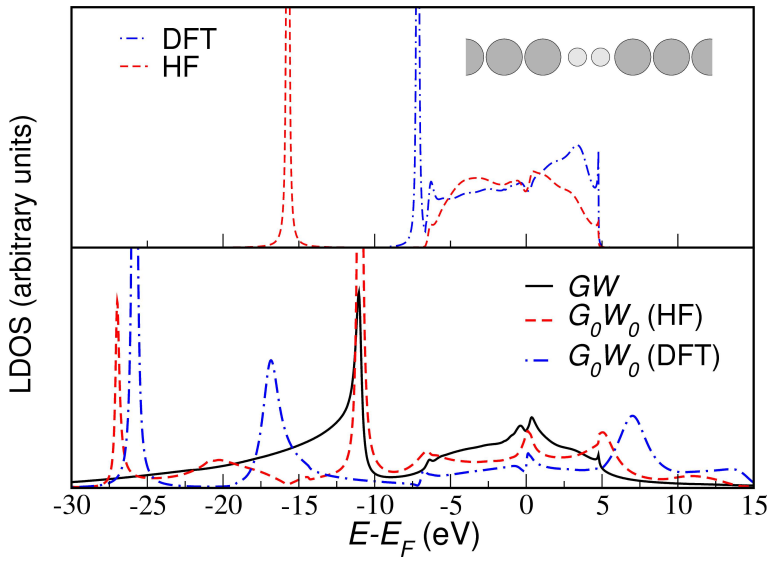

Figure 19: Local density of states at one of the H orbitals of the Pt-H-H-Pt contact shown in the inset. Reprinted with permission from K. S. Thygesen and A. Rubio, J. Chem. Phys. 126, 091101 (2007). Copyright 2007, American Institute of Physics.

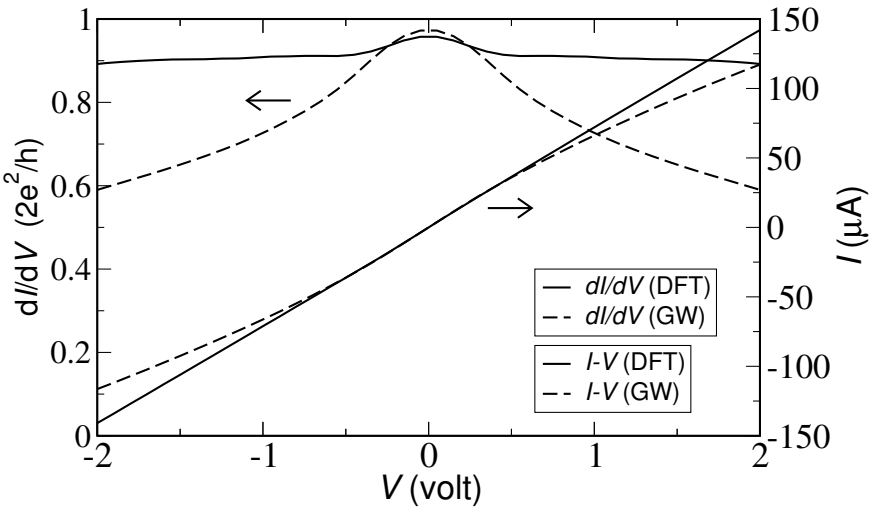

Figure 20: I-V and dI/dV for the hydrogen contact as calculated in DFT(PBE) and self-consistent GW. V is the source-drain bias voltage. Reprinted with permission from K. S. Thygesen and A. Rubio, J. Chem. Phys. 126, 091101 (2007). Copyright 2007, American Institute of Physics.

We are, however, aware that part of this large difference could be due to the limited size of the basis. We also mention that the LDOS results of Fig. 19 can be largely reproduced by

including only the second-order GW diagram in the self-energy. Thus the higher-order RPA diagrams are less important in this case.

In Fig. 20 we show the self-consistently calculated IV characteristics in DFT and GW. At low bias both schemes yield a conductance close to the experimental value of $1G_0$. The DFT conductance is nearly constant over the bias range, and is in fact very similar to the HF result (not shown). In contrast the GW conductance falls off at larger bias. This is due to enhancement of quasi-particle scattering at finite bias. The QP scattering reduces the life time of the QPs leading to broadening of the spectral peak associated with the anti-bonding state of the hydrogen molecule in agreement with the results for he two level model discussed in section 5.3. Since the correlation induced life-time of QP at the Fermi level, $\mathrm{Im}\Sigma_{\mathrm{corr}}(E_F)$, vanishes identically in equilibrium, the finite-bias conductance suppression seen in figure 20 is a direct result of the non-equilibrium treatment of correlations.

7 SUMMARY AND PERSPECTIVES

The feasibility of using many-body perturbation theory in combination with the Keldysh Green's function formalism to address nonequilibrium quantum transport through an interacting region coupled to non-interacting leads has been demonstrated. The effect of electronic correlations was incorporated into the Green's function via the GW self-energy, and the coupling to leads was treated exactly (to all orders in the hopping between leads and central region). The important connection between self-consistency in the GW self-energy and charge conservation was emphasized, and it was demonstrated that a non self-consistent treatment of the GW self-energy (the G_0W_0 approach) violates the continuity equation and produce unphysical results at finite bias. This, together with the arbitrariness of the G_0W_0 approximation due to its G_0-dependence, speaks in favor of the self-consistent GW approach to nonequilibrium transport.

The role of dynamic correlation effects in quantum transport was illustrated by applying the GW-transport scheme to a generic two-level model, a benzene molecule between featureless leads, and a hydrogen molecule between infinite Pt chains. It was shown that dynamic polarization of the leads as well as the molecule itself can lead to significant reduction of the molecule's HOMO-LUMO gap. The polarization effects were found to increase with the bias voltage where also quasiparticle scattering is strongly enhanced leading to broadening of the molecular resonances. As was shown, all these effects can have a large impact on the calculated IV curve. This should always be kept in mind, when interpreting results of meanfield (DFT or Hartree-Fock) transport calculations – in particular under finite bias.

As mentioned in the introduction, the quantitative theoretical description of quantum transport in nano-scale structures from first principles is an extremely complex problem. Nevertheless, simulations methods with predictive power are required to advance the field further. It has been known for several years that the standard DFT-NEGF scheme fails to predict even the zero-bias conductance of certain classes of systems. This state of affairs makes it difficult, although not impossible, to link theory and experiments and thereby stimulate the development of nano-scale electronics.

As illustrated by the examples given in this chapter, reliable schemes for quantum transport should account for dynamic correlation effects in some way or another. The *GW* method discussed here includes some correlation effects, but misses others, e.g. the side peaks in the spectral function of the Anderson model are not well reproduced (Thygesen and Rubio 2007). Methods developed for strongly correlated systems, such as density matrix renormalization group theory (Schmitteckert and Evers 2008), are limited to simple models due to their inexpedient scaling with system size. The effective single-particle scheme of TDDFT makes it an attractive alternative to many-body perturbation theory, in particular for dynamical transport phenomena (Stefanucci *et al.* 2007). However, the inclusion of correlation effects requires use of xc-potentials with memory which have so far proved difficult to construct.

Another important aspect of the problem is related to the coupling between electrons and nuclei. Despite the large difference in the general time scales of electronic and nuclear motions, electronic wavepackets quite often couple with the dynamics of nuclear motion (Frederiksen *et al.* 2004, Verdozzi *et al.* 2006). The proper incorporation of the electronic-nuclear interaction is crucial for describing a host of dynamical processes including Joule heating, electromigration, laser-induced electronic transport and electron transfer in molecular, biological, or electrochemical systems. Within the groundstate DFT framework, the computation of forces on the nuclei is trivial thanks to the Hellman-Feynman theorem. The situation is more complex out of equilibrium, and even more so in combination with a many-body description of the electrons, where the Hellman-Feynman theorem does not apply. However, the electron-ion dynamics must eventually be taken properly into account for a realistic description of a large class of molecular devices relevant for technological applications such as fast, integrated, optoelectronic nanodevices.

ACKNOWLEDGMENTS

KST acknowledges support from the Danish Center for Scientific Computing through grant No. HDW-1103-06 and The Lundbeck Foundation's Center for Atomic-scale Materials Design (CAMD). AR acknowledge funding by the Spanish MEC (FIS2007-65702-C02-01), "Grupos Consolidados UPV/EHU del Gobierno Vasco" (IT-319-07), and by the European Community through NoE Nanoquanta (NMP4-CT-2004-500198), e-I3 ETSF project (INFRA-2007-1.2.2: Grant Agreement Number 211956) SANES(NMP4-CT-2006-017310), DNA-NANODEVICES (IST-2006-029192) and NANO-ERA Chemistry projects and the computer resources provided by the Barcelona Supercomputing Center, the Basque Country University UPV/EHU (SGIker Arina).

APPENDIX

Let $B(\tau,\tau')$ and $C(\tau,\tau')$ be two matrix valued functions on the Keldysh contour, and consider the commutator A defined by

$$A(\tau,\tau') = \int_{\mathcal{C}} [B(\tau,\tau_1)C(\tau_1,\tau') - C(\tau,\tau_1)B(\tau_1,\tau')]\mathrm{d}\tau_1, \tag{92}$$

where matrix multiplication is implied. Under steady state conditions where the real time components of B and C can be assumed to depend only on the time difference $t'-t$, the

following identity holds:

$$\mathrm{Tr}[A^<(t,t)] = \int \frac{\mathrm{d}\omega}{2\pi} \mathrm{Tr}[B^<(\omega)C^>(\omega) - B^>(\omega)C^<(\omega)]. \tag{93}$$

To prove this relation we first use the Langreth rules to obtain

$$\begin{aligned} A^<(t,t') &= \int \big[B^<(t,t_1)C^a(t_1,t') + B^r(t,t_1)C^<(t_1,t') \\ &- C^<(t,t_1)B^a(t_1,t') - C^r(t,t_1)B^<(t_1,t')\big]\mathrm{d}t_1. \end{aligned}$$

Since all quantities on the right hand side depend only on the time difference we identify the integrals as convolutions which in turn become products when Fourier transformed. We thus have

$$\begin{aligned} A^<(t,t) &= \int \frac{\mathrm{d}\omega}{2\pi} A^<(\omega) \\ &= \int \frac{\mathrm{d}\omega}{2\pi} [B^<(\omega)C^a(\omega) + B^r(\omega)C^<(\omega) \\ &\quad -C^<(\omega)B^a(\omega) - C^r(\omega)B^<(\omega)]. \end{aligned}$$

Eq. (93) now follows from the cyclic property of the trace and the identity $G^r - G^a = G^> - G^<$.

REFERENCES

Anderson, P.W. (1961) Phys. Rev. 124 41.
Bahn, S. R. and Jacobsen, K. W. (2002) Comp. Sci. Eng.4 56.
Baym, G. (1962), Phys. Rev. 127 1391.
Baym, G., and Kadanoff, L. P. (1962) Phys. Rev. 124 287.
Bokes, P., Jung, J., Godby, R. W. (2007) Phys. Rev. B 76 125433.
Brandbyge, M., Mozos, J. L., Ordej0n, P., Taylor, J., and Stokbro, K. (2002) Phys. Rev. B 65 165401.
Coleman, P. (1984) Phys. Rev. B 29 3035.
Costi, T. A., Hewson, A. C. and Zlatic V. (1994) J. Phys. Cond. Matt. 6 2519.
Cuniberti, G., Fagas, G., and Richter, K. (2005) *Introducing molecular electronics*, Springer.
Datta, S. (1995) *Electronic Transport in Mesoscopic Systems*, Cambridge University Press.
Delaney, P., Greer, J. C. (2004) Phys. Rev. Lett. 93 036805.
Di Ventra, M., Todorov, T. N. (2004) J. Phys.:Condens. Matter 16 8025.
Dubois, M., Latil, S., Scifo, L., Grvin, B., and Rubio, A. (2006), J. Chem. Phys. 125 34708-9.
Frederiksen, T., Brandbyge, M., Lorente, N., and Jauho, A.-P. (2004) Phys. Rev. Lett. 93, 256601.
García-Suárez, V. M., Rocha, A. R., Bailey, S. W., Lambert, C. J., Sanvito, S., and Ferrer, J. (2005), Phys. Rev. Lett. 95 256804.
Goldhaber, -G. D., Shtrikman, H., Mahalu, D., Abusch-Magder, D., Meirav, U. and Kastner, M. A. (1998) Nature 391 156.
Haug, H. and Jauho, A.-P. (1998) *Quantum Kinetics in Transport and Optics of Semiconductors*, Springer.
Hershfield, S., Davies, J.H. and Wilkins J. W. (1991) Phys. Rev. Lett. 67 3720.
Hettler, M. H., Wenzel, W., Wegewijs, M. R., Schoeller, H. (2003) Phys. Rev. Lett. 90 076805.
Heurich, J., Cuevas, J. C., Wenzel, W. and Schon, G. (2002) Phys. Rev. Lett. 88 256803.
Hybertsen, M. S. and Louie, S. G. (1986) Phys. Rev. B 34 5390.
Joachim, C., Gimzewski, J. K., Aviram, A. (2000) Nature 408, 541.
Johnson, P. D., and Hulbert, S. L. (1987), Phys. Rev. B 35 9427.
Kubatkin, S., Danilov, A., Hjort, M., Cornil, J., Bredas, J.-L., Stuhr-Hansen, N., Hedeård, P., and Bjørnholm, T. (2003), Nature 425, 698.
Landauer, R. (1970), Phil. Mag. 21 863.
Leeuwen, R. van, Dahlen, N.E., Stefanucci, G., Almbladh, C.O. and Barth, U. von (2006) *Time-Dependent Density Functional Theory*, Springer.
Meir, Y. and Wingreen, N. S. (1992), Phys. Rev. Lett. 68 2512.
Mowbray, D. J., Jones, G., and Thygesen, K. S. (2008), J. Chem. Phys. 128 111103.
Neaton, J. B., Hybertsen, M. S., and Louie, S. G. (2006), Phys. Rev. Lett. 97 216405.
Nelson, W., Bokes, P., R. Patrick, and Godby, R.W. (2007) Phys. Rev. A 75 032505.
Niehaus, T. A., Rohlfing, M., Della, F. S., Di Carlo, A., Frauenheim, T. (2005) Phys. Rev. A 71 022508.
NIST Chemistry WebBook, http://webbook.nist.gov/chemistry/
Nygard, J., Cobden, D.H., Lindelof, P.E. (2000) Nature 408 342-6.
Onida, G., Reining, L., and Rubio, A. (2002), Rev. Mod. Phys. 74 601.
Perdew, J. P., Burke, K., and Ernzerhof, M. (1996), Phys. Rev. Lett. 77 3865.

Pulay, P. (1980) Chem. Phys. Lett. 73 393.
Quek, S. Y., Venkataraman, L., Choi, H. J., Louie, S. G., Hybertsen, M. S., and Neaton, J. B. (2007), Nano Lett. 7 3477.
Reichert, J., Ochs, R., Beckman, D., Weber, H. B., Mayor, M. and Löhneysen, H. (2002) Phys. Rev. Lett. 88 176804.
Repp, J., Meyer, G., Stojkovic, S. M., Gourdon, A., and Joachim, C. (2005), Phys. Rev. Lett. 94 026803.
Smit, R. H. M.,Noat, Y., Untiedt, C., Lang, N. D., Hemert, M. C., and Ruitenbeek, J. M. (2002) Nature 419 906.
Schmitteckert, P., Evers, F. (2008) Phys. Rev. Lett. 100, 086401.
Spataru, C. D, Benedict, L. X., and Louie, S. G. (2004), Phys. Rev. B 69 205204.
Stan, A., Dahlen, N. E., and Leeuwen, R. van (2006), Europhys. Lett. 76 298.
Stefanucci, G., Kurth, S., Gross, E. K. U., Rubio, A. (2007) Ed. J. Seminario 17 247 -284.
Taylor, J., Guo, H., and Wang, J. (2001) Phys. Rev. B 63 245407.
Thygesen, K. S. (2008), Phys. Rev. Lett. 100 166804.
Thygesen, K. S. (2006) Phys. Rev. B 73 035309.
Thygesen, K. S. and Jacobsen, K. W. (2005) Phys. Rev. Lett. 94 036807.
Thygesen, K.S. and Rubio, A. (2007), J. Chem. Phys. 126 091101.
Thygesen, K.S. and Rubio, A. (2008), Phys. Rev. B 35 9427.
Toher, C., Filippetti, A., Sanvito, S., and Burke, K. (2005), Phys. Rev. Lett. 95 146402.
Vanderbilt, D. (1990), Phys. Rev. B 41 7892.
Verdozzi, C., Godby, R. W., and Holloway, S. (1995), Phys. Rev. Lett. 74 2327.
Verdozzi, C., Stefanucci, G., Almbladh, C.-O. (2006) Phys. Rev. Lett. 97, 046603.
Wilson, K.G. (1975) Rev. Mod. Phys. 47 773.